Intracochlear pressure measurements related to cochlear tuning

Elizabeth S. Olson
Physics Department, Princeton University, Princeton, New Jersey 08544

(Received 14 November 2000; accepted for publication 7 March 2001)

Pressure in turn one of the scala tympani (s.t.) was measured close to the basilar membrane (b.m.) and at additional positions as the pressure sensor approached and/or withdrew from the b.m. The s.t. pressure measured within about 100 μm of the b.m. varied rapidly in space at frequencies around the region's best frequency. Very close to the b.m. the s.t. pressure was tuned and scaled nonlinearly with sound level. The scala vestibuli (s.v.) pressure was measured at one position close to the stapes within seconds of the s.t. pressure and served primarily as a reference pressure. The driving pressure across the organ of Corti and the b.m. velocity were derived from the pressure data. Both were tuned and nonlinear. Therefore, their ratio, the specific acoustic impedance of the organ of Corti complex, was relatively untuned, and only subtly nonlinear. The impedance was inspected specifically for negative resistance (amplification) and resonance. Both were detected in some instances; taken as a whole, the current results constrain the possibilities for these qualities. [DOI: 10.1121/1.1369098]

PACS numbers: 43.64.Kc [LHC]

I. INTRODUCTION

Basilar membrane (b.m.) motion is tuned and nonlinear (Rhode, 1971). Probing the mechanical basis for b.m. tuning and nonlinearity was the major objective of this work. The experimental strategy was to find the basilar membrane's motion and local driving pressure over a wide range of frequencies including the best frequency of the observation point. The driving pressure (the pressure difference across the organ of Corti complex, defined to include the organ of Corti and the basilar and tectorial membranes) was estimated according to cochlear-mechanical theory by combining intracochlear pressure measurements in the scala tympani (s.t.) close to the b.m. with measurements of the scalar vestibuli (s.v.) pressure near the stapes. The b.m. velocity was estimated from measurements of the s.t. pressure gradient near the b.m. The primary observation was that the driving pressure was tuned and nonlinear to nearly the same degree as b.m. motion. This observation speaks for the global nature of tuning in the mammalian cochlea, which sets it apart from hearing organs in which local tuning mechanisms, e.g., electrical resonances in turtle hair cells (Crawford and Fettiplace, 1981), mechanical resonances of the stereociliary bundles of alligator lizard hair cells (Freeman and Weiss, 1990) have been observed or inferred to be dominant. It is notable that in previous results from the extreme basal region the driving pressure appeared to be tuned substantially less sharply than b.m. motion (Olson, 1998). This difference between the extreme base and turn one is discussed at the end of Sec. VI B, impedance results.

The specific mechanical impedance of the organ of Corti complex (OCC) is equal to driving pressure divided by b.m. velocity. The impedance was found and inspected specifically for negative resistance and a spring-mass resonance. These qualities are fundamental to many models of cochlear operation—the resonance to peak the cochlear traveling wave and then bring it to a full halt; negative resistance to enhance the peak at low levels (deBoer, 1984; Kolston, 2000). However, there is neither a consensus for these qualities in cochlear models nor decisive experimental evidence for them. The present results inform but do not resolve the matter. Negative resistance was observed but not in all measurements on healthy cochleae. A spring-mass resonance was apparent in the phase data of several experiments at frequencies just above the best frequency (b.f.) of the response, where it is expected to be. However, at frequencies above the b.f. the driving pressure difference was close to zero, which made the analysis of this frequency region susceptible to experimental inaccuracies. (Following common usage, a region's best frequency is the frequency for which b.m. motion peaks at low sound pressure levels.)

The pressure measurements here are unique in emphasizing spatial variations in pressure close to the sensory tissue. Intracochlear pressure close to the cochlear wall has been measured to investigate the forward and reverse transfer functions of the middle ear (Nedzelnitsky, 1980; Dancer and Franke, 1980; Puria and Rosowski, 1997; Magnan *et al.*, 1999; Puria *et al.*, 1997; Decory *et al.*, 1990; Olson and Cooper, 2000), the cochlear input impedance (Lynch *et al.*, 1982; Aibara *et al.*, 1999) and distortion products (Magnan *et al.*, 1997; Avan *et al.*, 1998). Intracochlear pressure was measured in several turns and/or both scalae by Dancer and Franke (1980) and Nedzelnitsky (1980).

II. METHODS

The methods of this study were similar to those of Olson (1998) and are described in more detail there.

A. Pressure sensor construction and calibration

A pressure sensor consists of a glass capillary (inner and outer diameters 100 and 170 μm) tipped with a gold-coated polymer diaphragm. Light from an LED is delivered via an optic fiber threaded into the capillary, and reflects from the diaphragm. The amount of light retuning to the optic fiber for transmission to a photodetector varies linearly with the pressure-induced bending of the diaphragm. The acoustic

impedance of the sensors is at least an order of magnitude larger than that of the cochlea measured at the stapes.

Sensors were calibrated in water and air following assembly and in water before and after every experiment except in unusual cases in which a sensor broke. The difference between before and after calibrations was similar to what was reported previously. In the current experiments, the difference ranged from 0 to 6 dB, except experiment 12-10-98, for which the s.t. sensor calibration changed by 10 dB. For analysis, the average of the before and after calibrations was used. Calibration uncertainty was most detrimental when calculating the pressure difference across the OCC, because then the difference between two pressures measured with different sensors was taken. In a few experiments the s.t. sensor was swapped into s.v. or vice versa at the end in order to check the relative sensitivity of the sensors. A minority of sensors was found to be temperature sensitive. Therefore, following assembly, sensors were screened for temperature sensitivity and were not used if the variation with temperature between 26 °C and 38 °C was more than 3 dB.

B. Animal preparation

Animal procedures were approved by the Princeton University Institute Animal Care and Use Committee. The experimental animals were young adult mongolian gerbils (*Meriones unguiculatus*) 40–65 g in weight. Ketamine (40 mg/kg) was administered to sedate the animal, followed by the anesthetic sodium pentobarbital (initial dose 60 mg/kg). Supplemental smaller doses of sodium pentobarbital were given when deemed necessary from a toe pinch response, typically every half hour. The animal was deeply anesthetized throughout the procedure and then sacrificed with an overdose of anesthetic. The animal core temperature was maintained at 38 °C with an animal blanket. A small heater was attached to the head holder. The bulla was widely open during all data collection.

C. Sound system and calibration

Stimuli were generated and responses collected with a Tucker Davis Technologies DD1 using a 6.48 μs sampling period. The response to a click was collected and averaged with a LeCroy digital oscilloscope. Sound stimuli were produced with a Radio Shack tweeter and delivered to the ear canal via a closed sound system. In order to calibrate the stimulus, at the beginning of every experiment a pressure sensor was inserted into the ear canal via a small hole that was made in the bulla just in front of the tympanic membrane. The system was calibrated at up to 62 frequencies. In previous experiments the calibration hole was covered during and after calibration. In the current experiments that procedure was not followed without appreciable difference.

D. Intracochlear pressure measurements

In order to access the s.v. a hole just large enough for a pressure sensor was hand drilled through the bone basal to the oval window. The s.v. sensor was held in a micromanipulator and its tip was inserted 100–200 μm into the s.v. To access turn one of the s.t. a similar hole was hand drilled above the round window (r.w.) opening. Figure 1(a) shows the positions of the s.t. and s.v. holes. The s.t. sensor was positioned so that it was pointing as closely as possible toward the cochlear apex. An excised temporal bone and anatomical landmarks served as guides for positioning the s.t. sensor, which was tricky. A hole too close to the stapedial artery made it impossible to correctly angle the sensor and instead of the b.m., the spiral lamina was approached. This resulted in greatly reduced pressure gradients. A hole too far from the stapedial artery damaged the spiral ligament, ending an experiment. When the hole was all right, often several approaches were made at slightly different angles in order to change the longitudinal and/or lateral position of the sensor on the b.m. by 50–100 μm. In one of the experiments presented here, the s.t. pressure was measured in the extreme base. To access the extreme base of the s.t. the sensor was inserted through the r.w. opening following removal of the r.w. membrane.

The s.t. sensor was held in a micromanipulator capable of both manual and motorized positioning. The sensor was guided into the hole manually, and advanced within the hole using the motorized manipulator. Figure 1(b) illustrates the

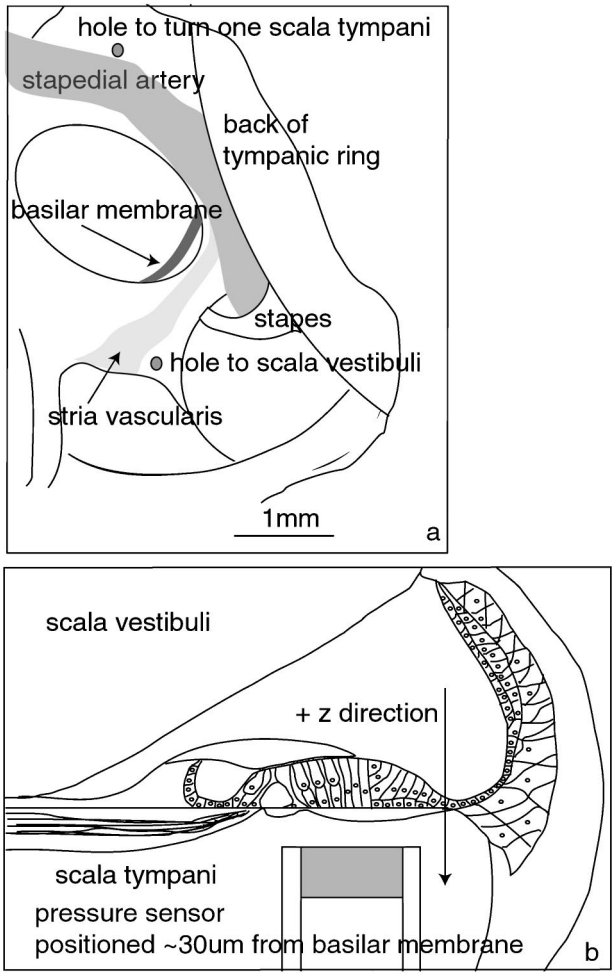

FIG. 1. (a) View of the cochlea during experiments. Not shown are the pressure sensors which were inserted into the s.v. and s.t. holes and the CAP electrode, which was positioned on the bone of the r.w. opening. (b) Idealized to-scale drawing of a pressure sensor positioned close to the b.m. in the s.t.

sensor positioned close to the b.m. When close to the b.m., measurements were usually spaced by 10 or 20 μm in the direction along the sensor axis (z axis). In later experiments the s.t. sensor was held in a piezoelectric bimorph assembly similar to that described in Olson and Mountain (1991), which in turn was held in the motorized manipulator. The bimorphs were driven with DC voltage in order to advance and retract the s.t. sensor in the direction along its axis. In these experiments at each frequency and level the s.t. pressure was measured consecutively at two positions separated by 12 μm. This procedural change was made in order to reduce the effect of slow changes (for example, in fluid level) on the calculation of fluid velocity. The distance from the b.m. was determined by touching it with the sensor, which produced a bouncy sensor response on the oscilloscope.

The pressure stimuli were pure tones, 32 ms in duration. The number of averages taken ranged from 20 to 200. The responses were stored and later analyzed via fast Fourier transform to find the magnitude and phase at the stimulus frequency. The initial 5 ms of the response was truncated before analysis in order to exclude the transient response. In one of the presented experiments the pressure stimulus was a click produced by driving the earphone with a 10 μs voltage pulse. Because of the frequency response of the speaker the acoustic pulse in the ear canal was longer than 10 μs.

E. Compound action potential

A silver wire electrode insulated to its tip was positioned on the bone near the r.w. This was used to measure the compound action potential (CAP) response to tones, as a monitor of cochlear condition (Johnstone *et al.*, 1979). CAP stimuli were tone bursts, 3 ms in duration. They ranged from 20 to 80 dB SPL in 10 dB increments and from 0.5 to 40 kHz at 10 or more frequencies. (SPL is decibels re 20 μPa.) Typically 60 responses were averaged. The polarity of alternate tones was reversed to reduce the cochlear microphonic in the averaged response. The averaged response was displayed on line and stored. ''Threshold'' CAP was defined as the visual threshold, 5 to 10 μV peak-to-peak.

III. RESULTS

In all the results, phases are shown referenced to the s.v. pressure phase measured at the stapes within seconds of each s.t. pressure measurement. The s.v. pressure at the stapes can be considered as the input pressure of the cochlea.

IV. GROUPED RESULTS

A. General description

In Fig. 2 scala tympani pressure magnitude and phase is shown from 14 turn one experiments. The stimulus level was 80 dB SPL in all cases, and these were initial data, taken with the s.t. sensor ~150 μm within the s.t., ~300 μm from the b.m. The average s.t. pressure is also shown, and the average s.v. pressure close to the stapes from these experiments. The character of the s.v. pressure was described previously (Olson, 1998), here it suffices to repeat that above 1

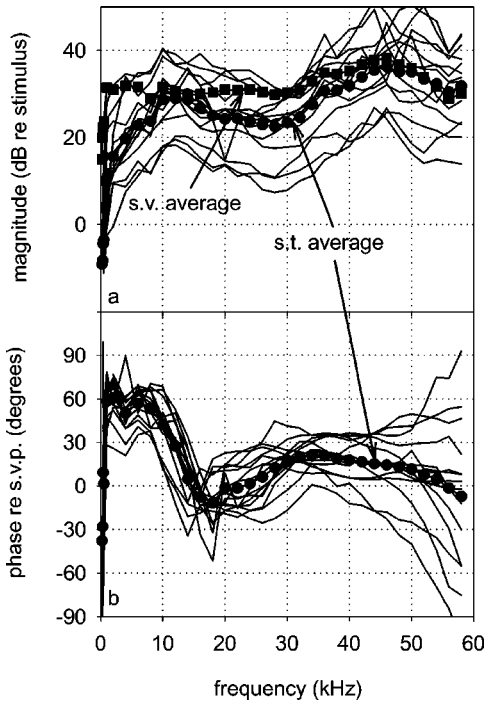

FIG. 2. Turn-one scala tympani pressures far from the b.m., 14 experiments. Also shown are the average of these measurements and the average of the s.v. pressures near the stapes from the same experiments. The stimulus level was 80 dB SPL in the ear canal. (a) Magnitude *re* stimulus level in ear canal. (b) Phase relative to the simultaneously measured pressure in s.v. near the stapes.

kHz the s.v. pressure scaled linearly (except as discussed at the end of Sec. IV B 2), and that it was nearly flat with frequency, with a gain relative to the ear canal pressure of ~30 dB. The s.t. phase is shown relative to the ~ simultaneously measured pressure in the s.v. Figure 3 shows the Fig. 2 s.t. data from the experiments that will be used in the impedance analysis, and include data from an extreme basal experiment. Referring to Fig. 2, the s.t. pressure was substantially smaller than the s.v. pressure at frequencies below 10 kHz, and had two broad peaks, centered at ~12 and 45 kHz. The lower frequency peak is just under the best frequency of this region. This peak and the phase drop between 10 and 20 kHz are likely manifestations of the traveling wave. Similar behavior occurred between 20 and 30 kHz in the extreme base (curve 2-26-97 of Fig. 3). The 45 kHz peak was also present in the s.v. pressure and might be due to a standing wave in the ear canal described in ''sound system calibration'' in Olson (1998).

The behavior of the extreme basal s.t. pressure (2-26-97 of Fig. 3) at frequencies well below the b.f. can be understood in terms of a lumped element model. The model is shown in Fig. 4 with element values in the caption. In the usual way (Beranek, 1954) mass is treated as an inductor and stiffness as a capacitor. m_v and m_t are the fluids in the s.v. and s.t. in the region between the cochlear windows. r_c is the ''transmission line'' resistance of the cochlea (Zwilslocki, 1965). The capacitor represents the stiffness of the basilar membrane in the immediate vicinity of the windows. The model is kept very simple; e.g., the mass and resistance associated with fluid flow through the helicotrema are not in-

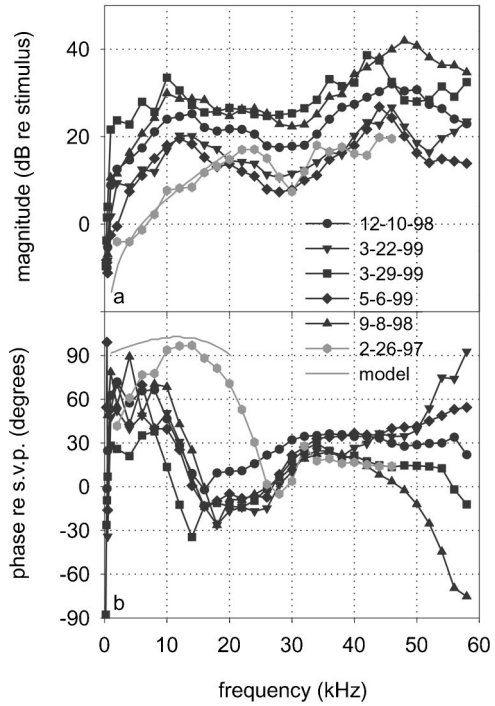

FIG. 3. Turn-one scala tympani pressures far from the b.m. Similar data as in Fig. 2, but only from those experiments used in the impedance analysis, and including an extreme basal measurement. The response of the lumped parameter model in Fig. 4 is included to shed light on the low frequency results.

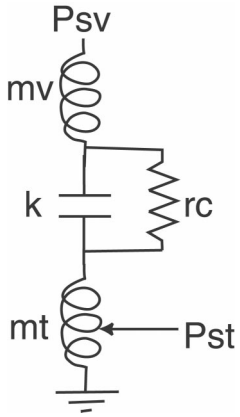

FIG. 4. Simple lumped parameter model of extreme base of cochlea at frequencies well beneath the region's best frequency. $P_{s.v.}$ is the pressure measured in the s.v. near the stapes. $P_{s.t.}$ is the extreme basal scala tympani pressure, measured about 100 μm within the s.t. fluid. The round window membrane was removed for measurements of extreme basal s.t. pressure and the sensor entered the s.t. through the r.w. opening. m_v and m_t are the fluid masses within the s.v. and s.t. in the basal region. They are taken to be equal with a value of 3.3×10^5 mks acoustic ohm s. [An acoustic ohm =pressure/volume velocity$=N/(\mathrm{m}^5/\mathrm{s})$.] This value is reasonable given the depth of the fluid column between the oval and round windows (~1 mm), and the sizes of the windows. r_c is the ''transmission line'' resistance of the cochlea, and its value of 1.7×10^{11} ohm is based on measurements of gerbil cochlear input impedance (Olson and Cooper, 2000). For comparison, Lynch *et al.* (1982) found a value of 1.2×10^{11} for r_c in cat. k is the stiffness of the OCC in the region between the oval and round windows. The stiffness value was found using the 4 Pa/nm value reported in Olson (1998) for the extreme basal OCC stiffness. Similar values were reported (as b.m. compliance) from a number of sources in Table IV of Ruggero *et al.* (1990), and the results presented later in this paper are also in reasonable accord with this value. The width of the OCC in this region is ~0.2 mm, and a length of ~1 mm is in the vicinity of the stapes. From these, the OCC stiffness was estimated as $\sim2\times10^{16}$ ohm/s.

cluded (Lynch *et al.*, 1982). Figure 3 shows the extreme basal s.t. pressure that the model predicts at a depth ~100 μm within the fluid of the s.t. In particular, the model explains how the interaction of fluid mass and basilar membrane stiffness can cause the phase of s.t. pressure re s.v. pressure to increase to a value greater than 90°. The model does not apply to the turn-one measurements, which were made some distance along the ''transmission line.'' (To model the turn one measurements r_c must be partly expanded into inductive and capacitive elements so the measurement position could be placed some distance along the transmission line.) Nevertheless, the well-below-b.f. turn-one results are fairly similar to the basal result, and can be loosely interpreted in a similar way.

B. Experimental uncertainties and perturbations

1. Exploring the variability

The spread of s.t. values in Fig. 2 is likely due to a combination of experimental conditions and calibration inaccuracies. The measurements rely on both the s.t. sensor and the ear canal sensor, so much of the ±12 dB variability in magnitude could be due to inaccurate calibration. An influential experimental condition is the fluid level in the r.w. opening. A higher fluid level caused an increase in the turn one s.t. pressure at frequencies above the b.f. In one experiment (7-13-98) the s.t. pressure around 40 kHz increased by ~10 dB when the r.w. opening was filled relative to when it was drained. At higher frequencies the effect was slightly less, and at frequencies below 23 kHz, the changes were ~2 dB. The s.t. pressure phases in Fig. 2(b) fan out at frequencies above 40 kHz. A 45° spread at 40 kHz grew to a 180° spread at 58 kHz. This spread *cannot* be traced to sensor variability. Comparing calibrations within experiments 3-22-99, 9-8-98, and 4-5-99 [which produced the most extreme phase in Fig. 2(b)] revealed a s.t. sensor calibration–s.v. sensor calibration difference of at most 8° at frequencies up to 40 kHz, and an overall maximum difference of 27°. The reason for the divergent high frequency phases is not known.

2. Perturbative effect of holes and sensors in the cochlea

The s.v. hole was expected to perturb cochlear mechanics more than the s.t. hole. This is because the s.t. hole was just above the r.w. and the effect of a small hole near such a large opening is expected to be minor relative to the effect of the s.v. hole near the stapes. In order to evaluate the effect of the s.v. hole, in several experiments the s.t. hole was made first and the pressure ~150 μm within the s.t. was measured before and after drilling the s.v. hole and inserting the s.v. sensor. The results are shown in Fig. 5, where the after–before differences in s.t. pressure magnitude and phase are shown for three experiments. The differences were rarely more than 2 dB in magnitude or 15° in phase.

The CAP response was also used to gauge the effect of introducing sensors into the cochlea. The CAP thresholds often increased at all frequencies after making the holes and

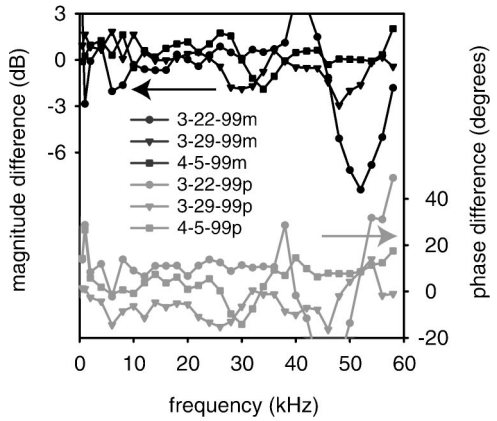

FIG. 5. Perturbation study: Change in the s.t. pressure after drilling the s.v. hole and inserting the s.v. sensor. Results from three experiments are shown. The magnitude changes (black lines) use the left axis, the phase changes (gray lines) use the right. The changes were small.

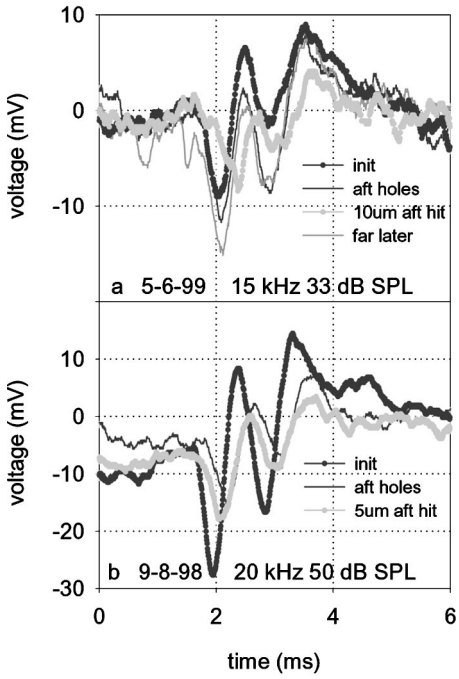

FIG. 6. Perturbation study using CAP response. CAP responses to a tone pip with frequency close to the b.f. of the longitudinal location under study were measured at various times. ''Init'' was the initial CAP, measured prior to drilling cochlear holes. ''Aft holes'' was after drilling the s.t. and s.v. holes and inserting the sensors. ''5 or 10 μm aft hit'' was the response when the s.t. sensor was 5 or 10 μm from the b.m., just after tapping it. ''Far later'' was after retracting the s.t. sensor. (a) Expt. 5-6-99. Here, the CAP response did not change upon introducing the sensors to the cochlea but was reversibly reduced when the s.t. sensor was close to the b.m. (b) Expt. 9-8-98. Here, the CAP response was reduced upon introducing the sensors to the cochlea but did not change further when the s.t. sensor was close to the b.m.

introducing the sensors. When the s.t. sensor was close to the b.m., further changes in the CAP response to tones at frequencies close to the b.f. sometimes occurred. Both these effects are illustrated in Fig. 6, which shows CAP responses to a tone close to the b.f. In the experiment of Fig. 6(a) (5-6-99), very little change occurred in the CAP following sensor introduction, but the CAP was reduced when the sensor was 10 μm from the b.m. The change was reversed when the sensor was retracted. In the experiment of Fig. 6(b) (9-8-98), the CAP response decreased after introducing the sensors, but was unchanged when the s.t. sensor was close to the b.m.

Another observation which bears on the influence of the sensor to cochlear mechanics is that the s.v. pressure measured at the stapes sometimes changed when the s.t. sensor was close to the b.m. The changes were largest at small sound levels and at frequencies close to the b.f. These changes were small, 3 dB at most, and reversible.

The conclusion drawn from these observations is that making holes and introducing sensors into the cochlea did not cause an overall reduction in the intracochlear pressure, but *usually* did traumatize the cochlea, leading to an overall decrease in sensitivity. When close to the b.m., the sensor sometimes perturbed cochlear mechanics.

V. SCALA TYMPANI PRESSURE VS POSITION

A series of pressure measurements made with spatial changes solely in the direction along the axis of the sensor is referred to as an approach. A ''run'' is a single run through of a data collection program, which comprises a series of frequencies and levels. When the piezoelectric positioner was in use, during a single run these data were collected at two positions in the s.t. which were separated by 12 μm in the z direction [see Fig. 1(b)]. In this section, approaches from the two best turn-one experiments, 9-8-98 and 5-6-99, are shown. Experiment 9-8-98 was performed before the piezoelectric positioner was in use; 5-6-99 did use the positioner. These experiments had relatively strong CAP responses, relatively strong compressive nonlinearity in s.t. pressure, stable fluid levels and repeatability of measurements over hours, especially 9-8-98. The basic observations are (i) the s.t. pressure close to the b.m. was tuned and compressively nonlinear, (ii) in some approaches the pressure variations close to the b.m. suggested that the distortion of the moving OCC was level dependent, and (iii) the pressure was composed of a sum of a traveling wave component which varied rapidly in space and a compressive component which varied very little in space. The last point is supported with an approach from a more recent experiment in which the pressure response to a click was measured.

This paragraph provides a brief guide to the figures in this section. Figure 7, from experiment 9-8-98, shows the s.t. pressure gain *re* ear canal pressure and the s.t. pressure phase re the simultaneously measured s.v. pressure at stimulus levels of 50 dB SPL (left panels) and 80 dB SPL (right panels). The measurements were made at distances ranging from 7 to 322 μm from the b.m. The complete approach included measurements at 13 positions. To improve figure clarity the data are not shown from every position. Figure 8 compares pre- and post-mortem data from 9-8-98. In Fig. 9 the results from an approach from experiment 5-6-99 are shown. For clarity only one of the intra-run positions (the closer of the two) is included in this figure. Responses were collected at 40, 50, 65, and 85 dB SPL, with the lower level responses collected over a narrower range of frequencies. The 50 dB SPL (left panels) and 85 dB SPL (right panels) results are in Fig. 9. Figure 10 shows magnitude data from the closest 5-6-99 run,

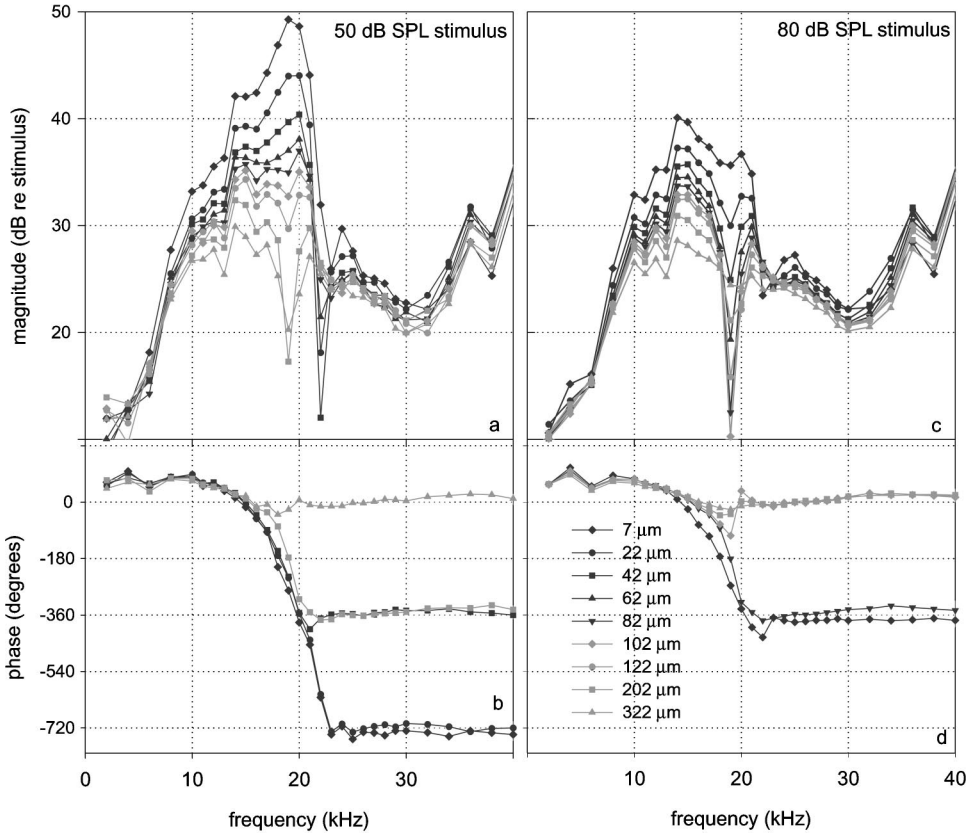

FIG. 7. The s.t. pressure as the s.t. sensor approached the b.m. Expt. 9-8-98. The key indicates the distance of the sensor from the b.m. To improve the clarity of the figures the phase data are shown at fewer positions than the magnitude data. Magnitudes are shown relative to the stimulus level in the ear canal; phases are relative to the simultaneously measured s.v. pressure. (a) Magnitude, 50 dB SPL stimulus. (b) Phase, 50 dB. (c) Magnitude, 80 dB. (d) Phase, 80 dB.

which is not included in Fig. 9 for the reason described in Sec. V C, at the two intra-run positions and all SPLs. Figure 11 shows the click response approach of experiment 4-25-00.

A. Nonlinearity

The similarity of Figs. 7 and 9 attests to the repeatability of the results in fairly healthy preparations. The results in Figs. 7, 9, and 10 show a moderate degree of compressive nonlinearity. For example, in Fig. 10, over the 40 to 85 dB range of stimulus levels the nonlinearity at the b.f. (18 kHz) was 20 dB. Nonlinearity began approximately a half octave below the b.f., at 12 kHz, and extended to just above the b.f., at 22 kHz. These nonlinear characteristics are similar to those reported for basal b.m. motion, although the degree of nonlinearity here was smaller than that of b.m. motion in the healthiest preparations (Ruggero *et al.*, 1997; Cooper, 1998; deBoer and Nuttall, 2000; Rhode and Recio, 2000). Based on the CAP thresholds even the best cochleae of this report were compromised slightly; this might account for the moderate level of compression. The data of Fig. 8 were taken just after those of Fig. 7, at a position 67 μm from the b.m. The pre-mortem data were taken, the animal was sacrificed with anesthetic, and the post-mortem data were taken minutes later. Nonlinearity disappeared post-mortem.

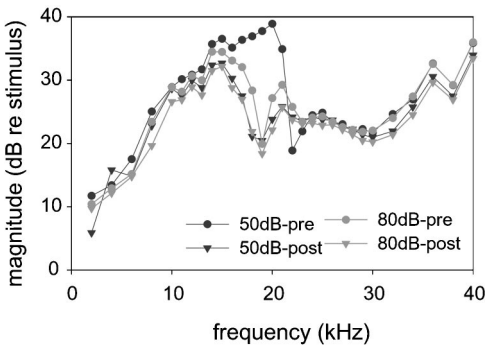

FIG. 8. The s.t. pressure magnitude re stimulus level measured at a distance 67 μm from the b.m. premortem and a few minutes postmortem. Expt. 9-8-98. Nonlinearity disappeared postmortem.

B. Suggestion of level dependent distortion of the organ of Corti

In the data of Fig. 9 the closest measurement *shown* was 20 μm from the b.m. The closest data run, 10 μm from the b.m., is not shown in Fig. 9 because, anomalously, the pressure was smaller at 10 than at 20 μm. This is illustrated in Fig. 10, which shows the pressure at the two intra-run positions of the closest run. The positions are 10 and 22 μm from the b.m. At 40 and 50 dB SPL and frequencies between the onset of nonlinearity and the b.f., the pressure at 22 μm was substantially bigger than at 10 μm. At 65 dB the effect was present but smaller. At 85 dB SPL the usual behavior, bigger pressure at the closer location, was observed. It is not difficult to imagine how the pressure at the closer location could be smaller than at the further location: For a simple beamlike radial profile of b.m. motion the pressure is greatest at the radial center (Steele and Taber, 1979). Ideally, the sensor approaches the radial center of the b.m. perpendicularly, as in Fig. 1(b). If the sensor approach is not quite perpendicular its degree of centering will change as it approaches. Then, when very close to hitting the b.m. the sensor could move from a region of relatively high pressure (more centered) to a

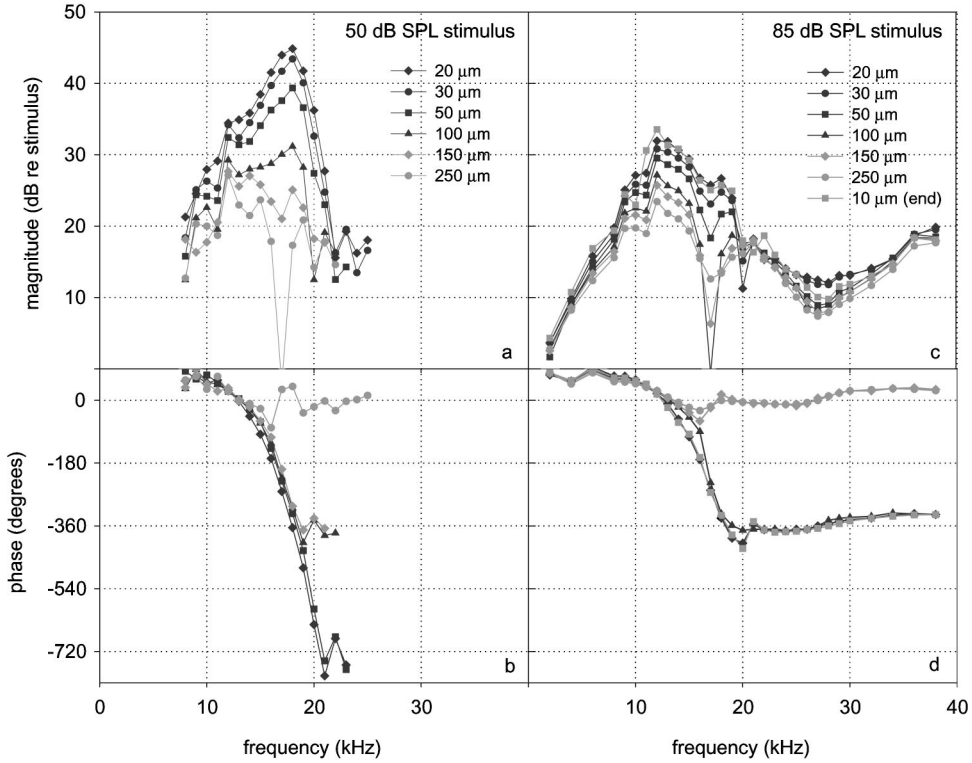

FIG. 9. The s.t. pressure as the s.t. sensor approached the b.m. Expt. 5-6-99. The key indicates the distance of the sensor from the b.m. To improve the clarity of the figures the phase data are shown at fewer positions than the magnitude data. Magnitudes are shown relative to the stimulus level in the ear canal; phases are relative to the simultaneously measured s.v. pressure. (a) Magnitude, 50 dB SPL stimulus. (b) Phase, 50 dB. (c) Magnitude, 85 dB. (d) Phase, 85 dB.

region of lower pressure (less centered). This effect was sketched in Olson (2000). What was intriguing about the reversal in the pressure gradient was that it sometimes depended on stimulus level, as in Fig. 10. This observation suggests that the radial profile of b.m. motion—in other words, the shape the b.m. took as it moved—underwent level dependent changes. The level dependent distortion could arise via a force generated from within the OC (e.g., Mountain and Hubbard, 1989; Kolston, 1999) whose strength was level dependent. In studies of the radial profile of basal b.m. motion, Cooper (2000) found a unimodal, beamlike profile of gerbil basal b.m. motion whose shape was mildly level dependent; the trimodal radial profile reported by Nilsen and Russell (1999) from the guinea pig base was also mildly level dependent. In the current study, level dependent reversals in pressure gradient occurred in several experiments, although not in experiment 9-8-98 or in a second approach of experiment 5-6-99. [Finally, the pressure sensor could be influencing the level dependence of the reversals. The perturbation of the sensor depends on the relative impedances of the sensor and the OCC. The frequency region just below the b.f. is implicated in cochlear amplification (e.g., deBoer and Nuttall, 2000 and see below), so the impedance in this region might be level dependent. Therefore, the perturbative effects of the sensor might be level dependent in this region.]

C. Multi-component nature of intracochlear pressure

Many aspects of the s.t. pressure reflect its being the sum of a traveling wave and a compressive wave. As background to this view: *The traveling wave pressure is produced by and produces the traveling wave motion of the* OCC. *It is largest near the* OCC *and spreads with decreasing amplitude into the scalae. The compressional pressure is produced by the compression of the cochlear fluid by the motion of the stapes and fills the cochlea approximately uniformly*. In this interpretation: (i) The phase accumulated at positions close to the b.m. because the traveling wave component is dominant there [Figs. 7 and 9, (b) and (d)]. (iii) The phase accumulated more at low stimulus levels because nonlinearity makes the traveling wave relatively stronger at low levels [Figs. 7 and 9, (b) and (d)]. (iii) The phase did not accumulate at frequencies above the peak because the traveling wave is small (perhaps nonexistent) relative to the compressional pressure there [Figs. 7 and 9, (b) and (d)]. (iv) Spatial variations, which register fluid motions, were large at frequencies of the peak because the fluid motions of the traveling wave are substantial (Figs. 7 and 9). (v) Spatial variations were small at frequencies above the peak because the fluid motions associated with the compressional wave are very small (Fig. 7). [In Fig. 9(c) the pressure *did* vary in space at frequencies above the peak. However, these changes were at least in part actually *time* dependent changes, as can be seen by comparing data collected with the sensor close to the b.m. at the beginning (20 μm position) and end of the approach (10 μm-end position).] (vi) Notches were caused by cancellation between traveling wave and compressional wave components [Figs. 7 and 9, (a) and (c)] (Cooper and Rhode, 1996).

Figure 11 also speaks for the two component nature of the pressure. It shows the response to a click (experiment 4-25-00, maximum level in the ear canal 77 dB) measured at several distances from the b.m. in the s.t. The initial peak of the response, which is presumably the compressional wave, did not change with position. In contrast, the ''slow'' ringing response, presumably the traveling wave, became more and more pronounced as the b.m. was approached.

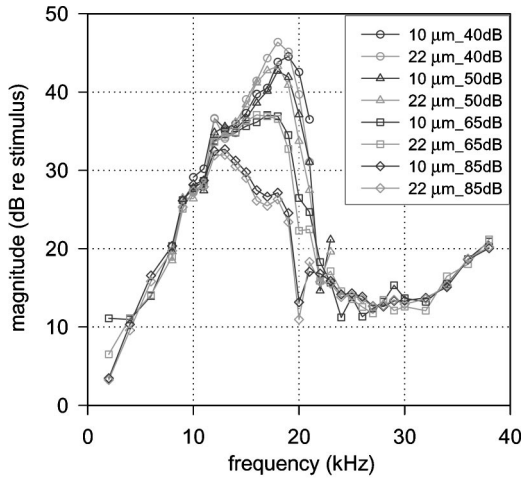

FIG. 10. The s.t. pressure magnitude *re* stimulus level 10 and 22 μm from the b.m. Expt. 5-6-99. These measurements were from the same approach as in Fig. 9; this was the closest position of that approach. The results here show level-dependent reversals in the relative magnitudes of the closer (10 μm) and farther (22 μm) pressures. Responses at 40, 50, 65, and 85 dB SPL are shown. At 85 dB SPL the pressure at the closer position was larger, as is usually the case. At 40, 50, and 65 dB SPL the pressure at the closer position was smaller over some portion of the left side of the response peak.

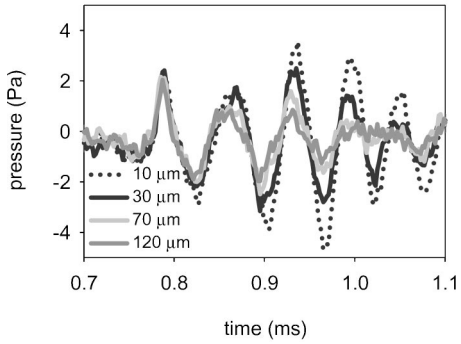

FIG. 11. The s.t. pressure response to a click measured at several distances from the b.m. Expt. 4-25-00. The click was produced by driving the earphone with a 10 μs voltage pulse, but filtering in the sound system produced a longer stimulus as measured in the ear canal. The key indicates the distance of the s.t. sensor from the b.m. The prolonged ringing response, presumably the traveling wave pressure, grew as the b.m. was approached, whereas the initial pressure peak, presumably the compressive pressure, remained almost the same.

VI. IMPEDANCE OF THE ORGAN OF CORTI COMPLEX

The specific acoustic impedance of the OCC (Z_{OC}) was derived from the pressure data. Z_{OC} is defined as the pressure across the OCC (ΔP_{OC}) divided by the *z* component of b.m. velocity ($v_{b.m.}$). [The *z* axis was defined in Fig. 1(b).]

In a passive system, Z_{OC} depends on the material properties and geometry of the OCC. For example, up to frequencies through the peak the passive part of Z_{OC} is likely, in simple terms, a combination of stiffness and damping. In an active system in which a force generator is present within the organ of Corti, that force, F_{active}, adds a term to the passive impedance which is equal to (F_{active}/area on which force acts)/$v_{b.m.}$. The Z_{OC} that these experiments find when the measured ΔP_{OC} is divided by the measured $v_{b.m.}$ is the sum of the passive part and the active part (deBoer and Nuttall, 2000). In cochlear models the active part is most successful at producing realistic b.m. tuning when it has the character of a negative damping that is large enough to cause the net damping to be negative over a limited region somewhat basal to the peak (e.g., deBoer, 1983; Neely and Kim, 1986; Kolston, 2000). *In the current experiments, performed at one place and many frequencies, this negative resistance would appear as a negative real part of the impedance at frequencies slightly below the b.f.*

In the classic traveling wave/resonant model of cochlear operation, the traveling wave, produced by the interaction of fluid inertia and OCC stiffness, ripples down the cochlear spiral. The decreasing stiffness of the OCC causes the traveling wave to slow and grow. At the point that the OCC mass begins to dominate its stiffness the traveling wave stops (e.g., Peterson and Bogart, 1950; Lighthill, 1981). The spring–mass transition is expected to occur slightly apical of the peak of the traveling wave. *Therefore, below and through the b.f. the imaginary part of the impedance is expected to be that of stiffness, and the spring–mass resonance will be looked for at frequencies slightly above the b.f. If the spring–mass resonance exists the imaginary part of the impedance will make a transition from stiffness dominated (negative) to mass dominated (positive) at the resonant frequency*.

A. Derivation

The analytic method for deriving ΔP_{OC} and $v_{b.m.}$ from the pressure measurements was described in Olson (1998). It is summarized here.

1. Basilar membrane velocity

The calculation of $v_{b.m.}$ uses one s.t. pressure measurement close to the b.m. (P_b) and a second s.t. pressure measurement a small distance from the first (P_a). The line that connects the two points of measurement is defined as the *z* direction, and it points away from the b.m., from the s.v. towards the s.t. [Fig. 1(b)].[1] At frequencies above a few kHz the *z* component of fluid velocity can be written very simply using these two pressures:

$$v_z \approx i(P_a - P_b)/(\omega \rho \Delta z). \tag{1}$$

In the expression, ω is the angular frequency, ρ is the density of the cochlear fluid, and Δz is the distance between the two pressure measurements. The fluid very close to the b.m. is expected to move with it, so when P_b is very close to the b.m. the fluid velocity approximates b.m. velocity. Then

$$v_{b.m.} \approx i(P_a - P_b)/(\omega \rho \Delta z). \tag{2}$$

2. Pressure across the organ of Corti complex

ΔP_{OC} is the pressure close to the OCC in the s.v. ($P_{s.v.-OCC}$) minus the pressure close to the b.m. in the s.t. (P_b). What was *measured* was the pressure in the s.v. near the stapes ($P_{s.v.}$) and the pressure in the s.t. close to the b.m. (P_b). With the simplifying assumptions that the cochlea is symmetric and the pressure at the r.w. is zero, $P_{s.v.} - P_{s.v.-OCC} = P_b - 0$, and

$$\Delta P_{OC} \approx P_{s.v.} - 2P_b \tag{3}$$

(see Footnote 2).

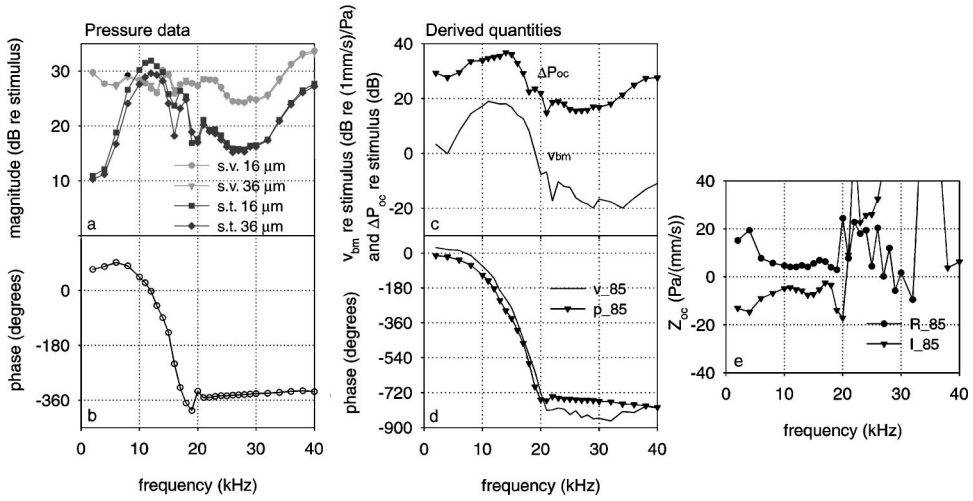

FIG. 12. Pressure data and derived quantities, 12-10-98. This was a nearly linear cochlea and only 85 dB SPL data are shown. (a) and (b) The s.t. and s.v. pressures for impedance calculation. Magnitude is shown relative to the stimulus level in the ear canal; phase (s.t. only) is relative to the simultaneously measured s.v. pressure. Distances in the key refer to the distance between the b.m. and the s.t. sensor. (a) Magnitude. (b) Phase. (c)–(e) ΔP_{OC}, $v_{\mathrm{b.m.}}$, and Z_{OC}. The usual calculation for ΔP_{OC} was used. (c) Magnitude of $v_{\mathrm{b.m.}}$ and ΔP_{OC} (*re* stimulus level). (d) Phase of $v_{\mathrm{b.m.}}$ and ΔP_{OC} (*re* simultaneously measured s.v. pressure). (e) Real and imaginary parts of Z_{OC}.

3. Specific acoustic impedance of the organ of Corti complex

$$Z_{\mathrm{OC}} = \Delta P_{\mathrm{OC}} / v_{\mathrm{b.m.}}. \tag{4}$$

B. Impedance results

Impedance results from six experiments are shown in Figs. 12–25. Impedances calculated for an additional six experiments are not shown because the results were noisier (due to time dependent variations or lower sensor sensitivity) and therefore less revealing than the six experiments that are presented. In each case the pressure measurements that went into the impedance calculation, the derived ΔP_{OC} and $v_{\mathrm{b.m.}}$ and the real and imaginary parts of Z_{OC} are plotted. Two introductory comments are in order: (1) The case-study presentation is fitting for communicating the impedance results because the meaning and authority of a particular Z_{OC} result is closely linked to the pressure measurements that generated it. Showing several case studies was necessary to demonstrate repeatability, variability, passive versus active, and turn one versus extreme base. (2) The weakest part of the analysis is the calculation of ΔP_{OC}. It was based on a symmetric cochlea, which could be an oversimplification. Further, it subtracts responses measured with two sensors, so even small calibration errors will introduce large errors when $P_{\mathrm{s.v.}} \approx 2P_b$. This weakness has been addressed by doing variations on the calculation, by finding ΔP_{OC} as $0.5P_{\mathrm{s.v.}} - 2P_b$ (contribution of s.v. pressure halved relative to usual calculation) and as $2P_{\mathrm{s.v.}} - 2P_b$ (contribution of s.v. pressure doubled) in a few cases. These variations show how a 6 dB calibration difference affects the impedance results and point out robust and fragile aspects of the results.

1. General conclusions

Taken as a whole the results lead to some general conclusions. From the ΔP_{OC} and $v_{\mathrm{b.m.}}$ plots: (i) The accumulation of the phases of both ΔP_{OC} and $v_{\mathrm{b.m.}}$ indicates that both are part of the cochlear traveling wave. (ii) Whether or not nonlinearity was present (i.e., in active and passive cochleae), both ΔP_{OC} and $v_{\mathrm{b.m.}}$ were tuned. (iii) When nonlinearity was in evidence it was usually present to nearly the same degree in both ΔP_{OC} and $v_{\mathrm{b.m.}}$. (An exception to this emerges from the analysis 9-8-98-I-double, as discussed below.) The Z_{OC} plots illustrate the relative and absolute sizes of the real and imaginary parts of the impedance, and indicate where it was stiffness dominated (imaginary part negative), mass dominated (imaginary part positive), and where the resistance was negative (real part negative). The Z_{OC} plots are most reliable in the broad region of the peak,

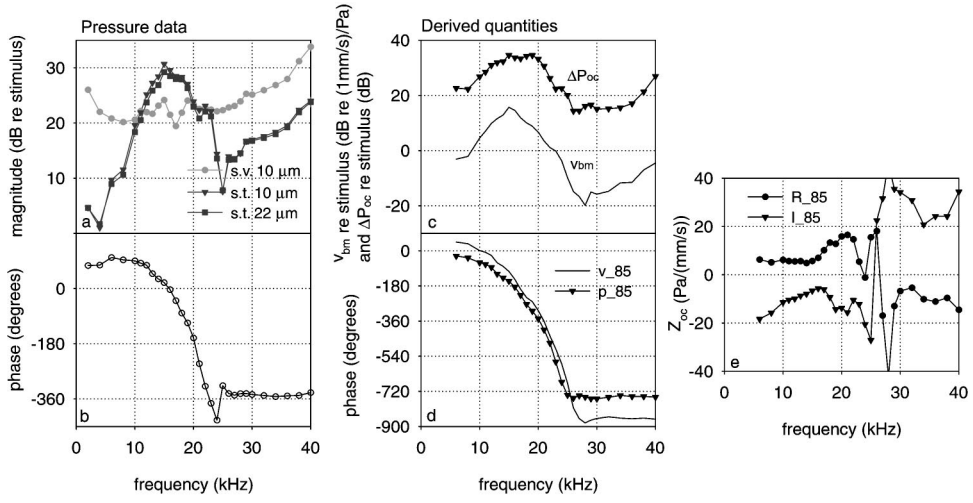

FIG. 13. Pressure data and derived quantities, 3-22-99. This was a nearly linear cochlea and only 85 dB SPL data are shown. (a) and (b) The s.t. and s.v. pressures for impedance calculation. Magnitude is shown relative to the stimulus level in the ear canal; phase (s.t. only) is relative to the simultaneously measured s.v. pressure. Distances in the key refer to the distance between the b.m. and the s.t. sensor. (a) Magnitude. (b) Phase. (c)–(e) ΔP_{OC}, $v_{\mathrm{b.m.}}$, and Z_{OC}. The usual calculation for ΔP_{OC} was used. (c) Magnitude of $v_{\mathrm{b.m.}}$ and ΔP_{OC} (*re* stimulus level). (d) Phase of $v_{\mathrm{b.m.}}$ and ΔP_{OC} (*re* simultaneously measured s.v. pressure) (e) Real and imaginary parts of Z_{OC}.

roughly 8–23 kHz (10–35 kHz for the extreme basal experiment 2-26-97), because there both the s.t. pressure and the spatial variations of the s.t. pressure were large. From these reliable regions of the plots, the additional general conclusions can be drawn: (iv) The imaginary part was negative (stiffness dominated) from low frequencies right up to and through the b.f. (v) In the ~5–10 kHz region (8–16 kHz for 2-26-97) the magnitude of the imaginary part usually decreased as frequency increased, as is expected for a stiffness. (vi) Overall, the real and imaginary parts were similar to each other in size; at 8–10 kHz they were mostly within 5–20 Pa/(mm/s) for the turn one experiments, and ~20 Pa/(mm/s) for the extreme basal experiment (2-26-97).

An additional general conclusion derives from the basic pressure data that introduces each case study, and bears on the calculation for ΔP_{OC}. Recall that ΔP_{OC} is found as $P_{s.v.} - 2P_b$. From the basic pressure data it is seen that at frequencies above the b.f. in the region of the phase plateau the s.t. pressure (P_b) was nearly in phase with the s.v. pressure and about 6 dB smaller. (The calibration uncertainty of ±6 dB makes this observation true within the uncertainty in all cases.) Therefore, the data are generally consistent with a ΔP_{OC} above the peak that is zero or close to it, which is true in most cochlear models. This is particularly pertinent to the investigation of spring–mass resonance.

2. Specific investigations

The six experiments were explored individually for (i) nonlinearity in the pressure data, (ii) evidence for negative resistance *below the b.f.*, and (iii) evidence for spring–mass resonance *closely above the b.f.* Table I, which appears at the end of the text, summarizes these results.

a. Spring–mass resonance. In the table, the ''detection'' of spring–mass resonance refers to an indication of spring–mass resonance in the phase. Resonance can be seen by inspecting the phase of $v_{b.m.}$ relative to ΔP_{OC}. A 90° lead indicates stiffness, a 90° lag indicates mass, (something less than 90° indicates resistance is present as well) and the transition from leading to lagging will occur at the resonance frequency. Alternatively, the imaginary part of Z_{OC} can be inspected—it will make a transition from negative to positive at the resonance frequency. Consider experiment 12-10-98 (Fig. 12). This cochlea was just barely nonlinear due to inadvertent damage to the cochlea. Therefore, only 85 dB SPL data are shown. The ΔP_{OC} phase began at 2 kHz at ~−10° with respect to the s.v. pressure, began to accumulate rapidly at 8 kHz, and leveled off at 20 kHz and ~−730°. The $v_{b.m.}$ phase went through a similar accumulation, but began by leading ΔP_{OC} by about 40°, crossed the ΔP_{OC} phase at 20 kHz, and leveled off at 21 kHz, lagging ΔP_{OC} by ~70°. The relative phase behavior suggests that Z_{OC} was stiffness and resistance dominated below 20 kHz, mass and resistance dominated above 20 kHz, and had a spring–mass resonance at 20 kHz. A spring–mass resonance is used in many cochlear models to bring the cochlear traveling wave to a halt, and the signature of a resonance just where the phase plateaus is compelling. Notably however, the magnitudes did not indicate a spring–mass resonance: the velocity did not peak relative to pressure at 20 kHz. The imaginary part of Z_{OC} from 12-10-98 of course tells the same story: the sign changed from negative to positive at ~20 kHz.

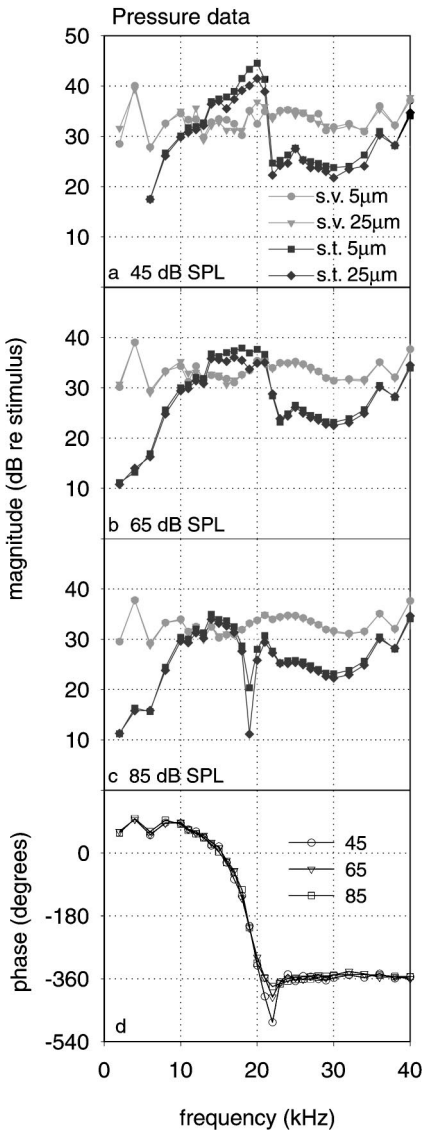

FIG. 14. Pressure data, 9-8-98-I. The s.t. and s.v. pressures for impedance calculation 9-8-98-I usual, 9-8-98-I-double and 9-8-98-I half. Magnitudes are shown relative to the stimulus level in the ear canal; phases (s.t. only) are relative to the simultaneously measured s.v. pressure. Distances in the key refer to the distance between the b.m. and the s.t. sensor. (a) Magnitude, 45 dB SPL stimulus. (b) Magnitude, 65 dB. (c) Magnitude, 85 dB. (d) Phase, all levels.

Experiment 3-22-99 (Fig. 13) was very similar to 12-10-98 and is shown primarily to demonstrate repeatability. The phases of $v_{b.m.}$ and ΔP_{OC} showed a similar course with frequency in the two experiments. In experiment 3-22-99 the resonance frequency indicated by the phase crossing was 25 kHz, which like 12-10-98 was slightly above the b.f. and at the beginning of the phase plateau. Similar to 12-10-98, 3-22-99 showed no sign of the resonance in the relative magnitudes of $v_{b.m.}$ and ΔP_{OC}. A difference in 3-22-99 compared to 12-10-98 is that in the final plateau $v_{b.m.}$ lagged ΔP_{OC} by slightly more than 90° (which indicates a component of negative resistance—unlikely in this linear cochlea, and suspected as an experimental error). Nevertheless, the

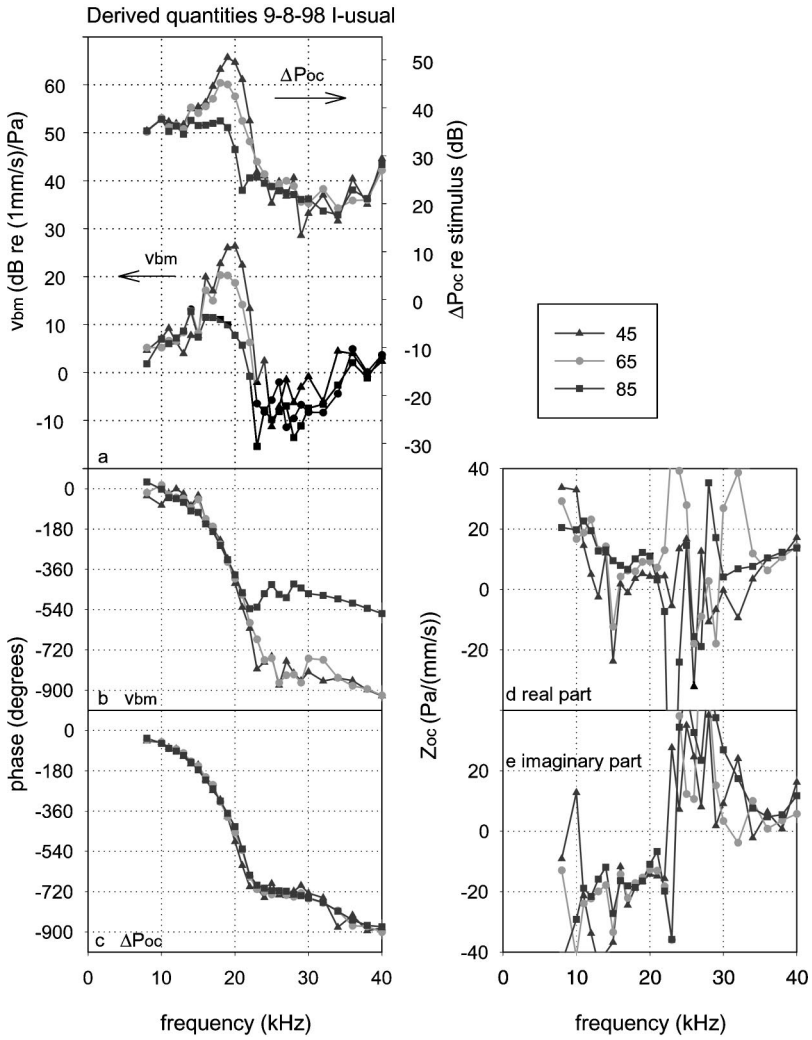

FIG. 15. Derived quantities ΔP_{OC}, $v_{b.m.}$, and Z_{OC}, 9-8-98-I-usual. The usual calculation for ΔP_{OC} was used. (a) Magnitude of $v_{b.m.}$ and ΔP_{OC} (*re* stimulus level). (b) Phase of $v_{b.m.}$ *re* simultaneously measured s.v. pressure. (c) Phase of ΔP_{OC} *re* simultaneously measured s.v. pressure. (d) Real part of Z_{OC} (e) Imaginary part of Z_{OC}.

phase data are close enough to looking like a spring–mass resonance to qualify for a yes in the table.

In the analysis of 9-8-98-I, ΔP_{OC} was calculated in the usual way and the two alternative ways, in which the contribution from s.v. pressure was halved or doubled. While spring–mass resonance was apparent in the phase of 9-8-98-I-usual (Fig. 15) and 9-8-98-I-double (Fig. 17), it was not apparent in the phase of 9-8-98-I-half (Fig. 16). The reason for the difference is that in 9-8-98-I-half at frequencies above the b.f. the s.t. pressure dominated the s.v. pressure in the calculation for ΔP_{OC} (Figs. 16 and 14, which shows the pressure data). Because of this the plateau level of the ΔP_{OC} phase changed by about 180° compared to the ΔP_{OC} phase for 9-8-98-I-usual and 9-8-98-I-double, causing the high frequency $v_{b.m.}$ to lead ΔP_{OC} by ~90° rather than lagging by ~90°. This comparison makes the point that, particularly in the plateau region, the calculated ΔP_{OC} can undergo large changes due to variations in s.v. and s.t. pressure that are within the experimental uncertainty.

On the spring–mass resonance question, the nonlinear experiment 5-6-99 (Fig. 19) is not helpful because it has an erratic $v_{b.m.}$ phase at frequencies above the b.f. Spring–mass resonance was not apparent in the analyses of experiments 3-29-99 and 2-26-97. $v_{b.m.}$ and ΔP_{OC} were nearly in phase at frequencies in the plateau region above the b.f. for 3-29-99-usual (Fig. 21), and $v_{b.m.}$ led ΔP_{OC} slightly in this region for 3-29-99-double (Fig. 22). In 2-26-97-usual (Fig. 24) and 2-26-97-half (Fig. 25) in the plateau region above the b.f. $v_{b.m.}$ led ΔP_{OC} by ~180°.

b. Negative resistance. Negative resistance was indicated when $v_{b.m.}$ led or lagged ΔP_{OC} by more than 90°. If present, it is expected at stimulus frequencies somewhat below the b.f., as these responses were passing through on the way to *their* b.f. place. For the purposes of ''detection,'' negative resistance must be in this region to be counted. (Strictly speaking negative resistance was often in evidence within the plateau region above the peak. However, the result was too erratic there to be trustworthy.) Negative resistance was cautiously detected in the two most nonlinear experiments, 5-6-99 and 9-8-98. To explore its character, consider experiment 9-8-98. 9-8-98-I (Figs. 15, 16, and 17) had a wiggle in the $v_{b.m.}$ phase and magnitude about half an octave below the b.f. The phase wiggle caused $v_{b.m.}$ to lead ΔP_{OC} by slightly more than 90° at 15 kHz. Therefore, negative resistance was indicated. Negative resistance appeared at 45 and 65, but not at 85 dB SPL for analyses 9-8-98-I-usual (Fig. 15) and 9-8-98-I-half (Fig. 16). In these cases both the frequency at which negative resistance appeared (slightly below the b.f.) and its level dependence (present at low levels,

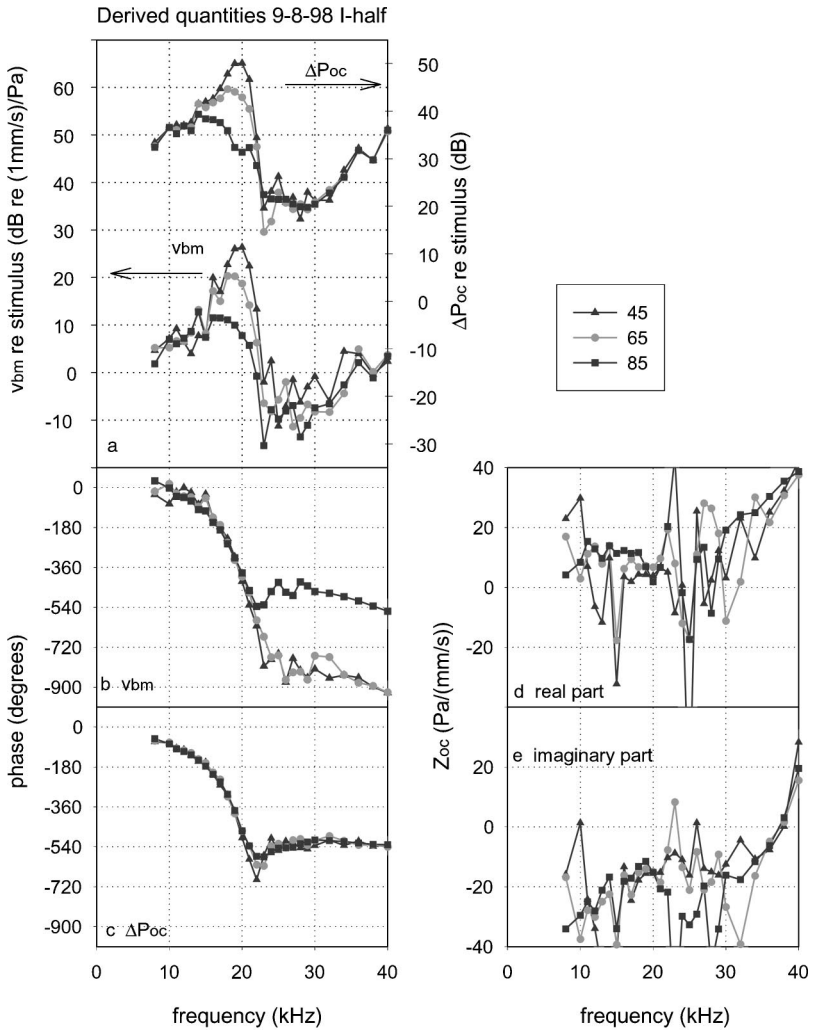

FIG. 16. Derived quantities ΔP_{OC}, $v_{b.m.}$, and Z_{OC}, 9-8-98-I-half. The contribution of $P_{s.v.}$ was half what it is in the usual calculation for ΔP_{OC}. (a) Magnitude of $v_{b.m.}$ and ΔP_{OC} (*re* stimulus level). (b) Phase of $v_{b.m.}$ *re* simultaneously measured s.v. pressure. (c) Phase of ΔP_{OC} *re* simultaneously measured s.v. pressure. (d) Real part of Z_{OC}. (e) Imaginary part of Z_{OC}.

absent at high levels) are consistent with model predictions. Negative resistance appeared at all three levels for 9-8-98-I-double (Fig. 17). Recall that in the ''double'' calculation, the contribution of s.v. pressure to the calculation of ΔP_{OC} was doubled. In the case of 9-8-98-I-double this variation has substantial effects. For one, the ΔP_{OC} phase found with the double calculation was less smooth than that found with the other calculations. This change is what caused the negative resistance to appear at all three levels. A second effect was that ΔP_{OC} was substantially less nonlinear than $v_{b.m.}$ so their ratio, Z_{OC}, *was* nonlinear. Negative resistance did not appear in 9-8-98-II (Fig. 18) a separate but equally nonlinear approach of this experiment. As can be seen in the pressure data from this approach, the s.t. pressure was relatively large in the region of the peak. Because of this, the s.t. pressure dominated s.v. in the calculation for ΔP_{OC}, and thus ΔP_{OC} was very similar in shape to $v_{b.m.}$. Therefore Z_{OC} was quite featureless, with little frequency change and no sign of negative resistance. 5-6-99 (Fig. 19) was similar to 9-8-98-I in that negative resistance was detected at low levels (40 and 50 dB, but not 65 and 85 dB) at a frequency about half an octave below the peak. Also similar to 9-8-98-I, the negative resistance stemmed from a wiggle in the velocity phase. None of the nearly linear experiments, 12-10-98, 3-22-99, and 2-26-97 showed negative resistance. In the analysis of the mildly nonlinear experiment 3-29-99, ΔP_{OC} was calculated in the usual way and with the s.v. contribution doubled. [The relative sizes of the s.v. and s.t. pressures in this experiment (Fig. 20) suggest that a calibration might have been in error and the 3-29-99-double analysis might be more accurate than the usual analysis.] ΔP_{OC} for 3-29-99-usual (Fig. 21) showed a sharp notch at 15 kHz and 85 dB SPL, which stems from a notch in the s.t. pressure. In 3-29-99-usual negative resistance was apparent only in the region of the notch. The level where negative resistance was apparent and the observation that it is related to a notch in ΔP_{OC} make it suspicious as an analytical error. In 3-29-99-double (Fig. 22), negative resistance was not apparent.

c. Extreme base compared to turn one. In gerbil the extreme basal region of the OCC is sandwiched between the cochlear windows, where it would be directly exposed to evanescent pressure modes (Steele and Taber, 1979). Because of this anatomy it is reasonable to expect that the results, particularly of ΔP_{OC}, would differ in the extreme base compared to turn one. It is notable that in healthy (chinchilla) cochleae the character of b.m. motion is quite similar in the extreme base and turn one (Narayan and Ruggero, 2000; Rhode and Recio, 2000).

2-26-97 was an extreme basal experiment, and was dis-

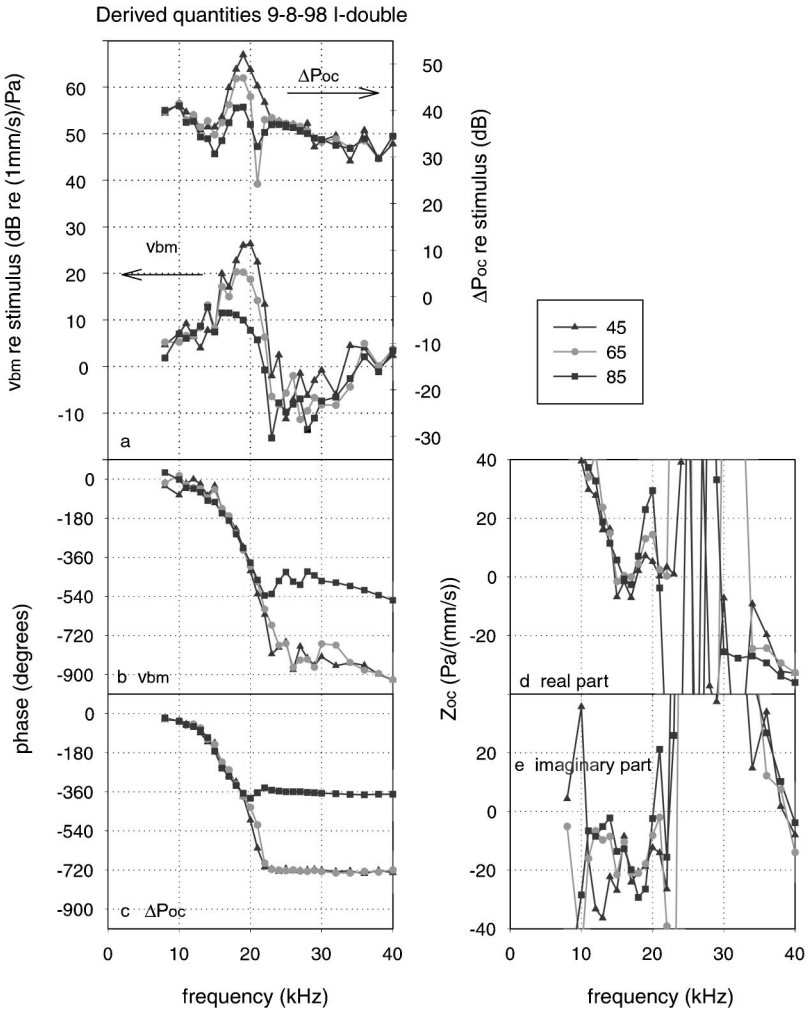

FIG. 17. Derived quantities ΔP_{OC}, $v_{b.m.}$, and Z_{OC}, 9-8-98-I-double. The contribution of $P_{s.v.}$ was twice what it is in the usual calculation for ΔP_{OC}. (a) Magnitude of $v_{b.m.}$ and ΔP_{OC} (*re* stimulus level). (b) Phase of $v_{b.m.}$ *re* simultaneously measured s.v. pressure. (c) Phase of ΔP_{OC} *re* simultaneously measured s.v. pressure. (d) Real part of Z_{OC}. (e) Imaginary part of Z_{OC}.

cussed in Olson (1998). In addition to finding ΔP_{OC} in the usual way (2-26-97-usual) it was also found with the contribution from s.v. pressure halved (2-26-97-half). This variation was calculated because the s.v. pressure was bigger than the average in this experiment (Fig. 23), suggesting that the s.v. sensor calibration might be in error. In that case the 2-26-97-half analysis might be more accurate. The 2-26-97-usual and 2-26-97-half analyses showed substantial dissimilarities. $v_{b.m.}$, ΔP_{OC}, and Z_{OC} from 2-26-97-half (Fig. 25) were quite similar, just shifted up in frequency, to those quantities in turn-one of the linear cochleae 12-10-98 and 3-22-98 (Figs. 12 and 13). In contrast, ΔP_{OC} for 2-26-97-usual (Fig. 24) was just barely tuned. Because $v_{b.m.}$ *was* tuned, Z_{OC} for 2-26-97-usual was more sharply tuned than for any of the turn one experiments. Considering the dissimilarity in the -half and -usual results, more measurements are necessary to decide whether and how cochlear mechanics differs in the region of the windows compared with other locations.

VII. DISCUSSION: CONCLUSIONS, COMPARISONS AND OTHER STRATEGIES FOR MEASURING Z_{OC}

The primary observations of this report were that the pressure close to the sensory tissue was tuned, and that it possessed a degree of nonlinearity similar to that of b.m. motion. These points were evident both in the primary s.t. pressure data, and the derived ΔP_{OC}. Therefore a primary conclusion is that compared to b.m. motion, the impedance of the OCC is relatively untuned, and is nonlinear in a different, subtler way.

The specific question of whether the cochlea provides power amplification in the form of negative resistance proved difficult to answer decisively. The two best cochleae, 9-8-98 and 5-6-99, both exhibited a brief flare of negative resistance over a 1–2 kHz range (one to two data points) within a kHz of the frequency where nonlinearity started, ~half an octave below the b.f. However, negative resistance was not detected in a separate equally nonlinear run of 9-8-98 or in the more mildly nonlinear cochlea 3-29-99. This ambiguity suggests that amplification's signature in the pressure close to the b.m. might vary radially. To address this matter requires a smaller pressure sensor. In the literature the most direct probe of negative resistance is that of deBoer and Nuttall (e.g., 1999, 2000). They derived the OCC impedance with an inverse method by coupling basilar membrane motion data to a 3-dimensional model of the cochlear fluid and geometry. Nuttall and deBoer made measurements of the frequency response at a single location, then used scaling and the cochlear map to convert the measured frequency response into an inferred spatial response. ''Below the b.f.'' in this study corresponds to ''basal to the peak'' in their analy-

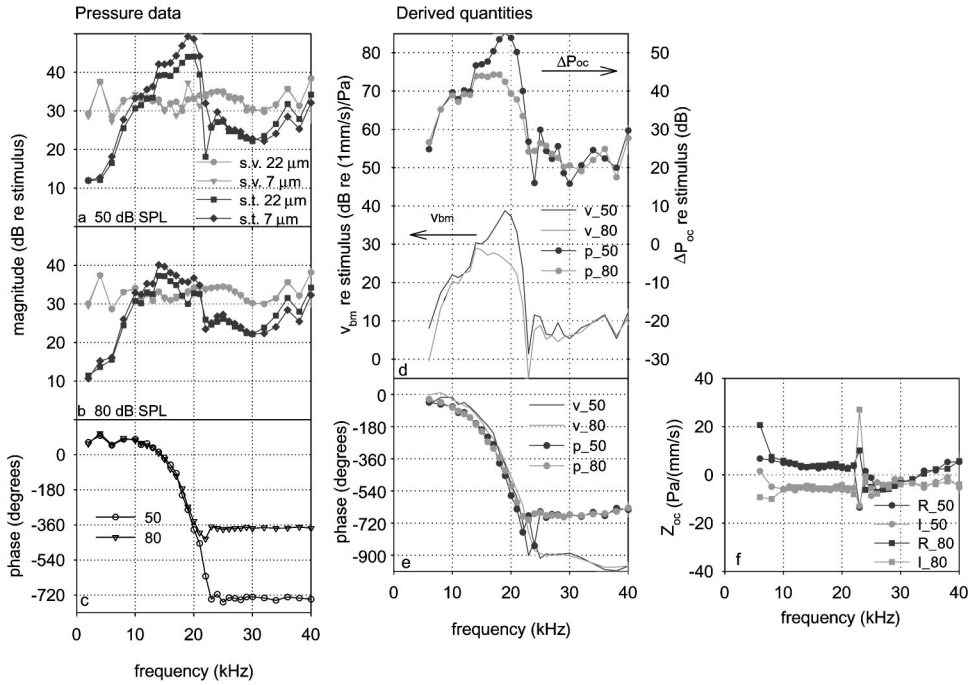

FIG. 18. Pressure data and derived quantities, 9-8-98-II. In approach 9-8-98-II the sensor was angled relative to 9-8-98-I by about 15° so that it would contact the b.m. ~100 μm from the first approach in a direction towards the lamina (a)–(c). The s.t. and s.v. pressures for impedance calculation. Magnitudes are shown relative to the stimulus level in the ear canal; phases (s.t. only) are relative to the simultaneously measured s.v. pressure. Distances in the key refer to the distance between the b.m. and the s.t. sensor. (a) Magnitude, 50 dB SPL stimulus. (b) Magnitude, 80 dB. (c) Phase, both levels. (d)–(f) ΔP_{OC}, $v_{b.m.}$, and Z_{OC}. The usual calculation for ΔP_{OC} was used. (d) Magnitude of $v_{b.m.}$ and ΔP_{OC} (*re* stimulus level). (e) Phase of $v_{b.m.}$ and ΔP_{OC} (*re* simultaneously measured s.v. pressure). (f) Real and imaginary parts of Z_{OC}.

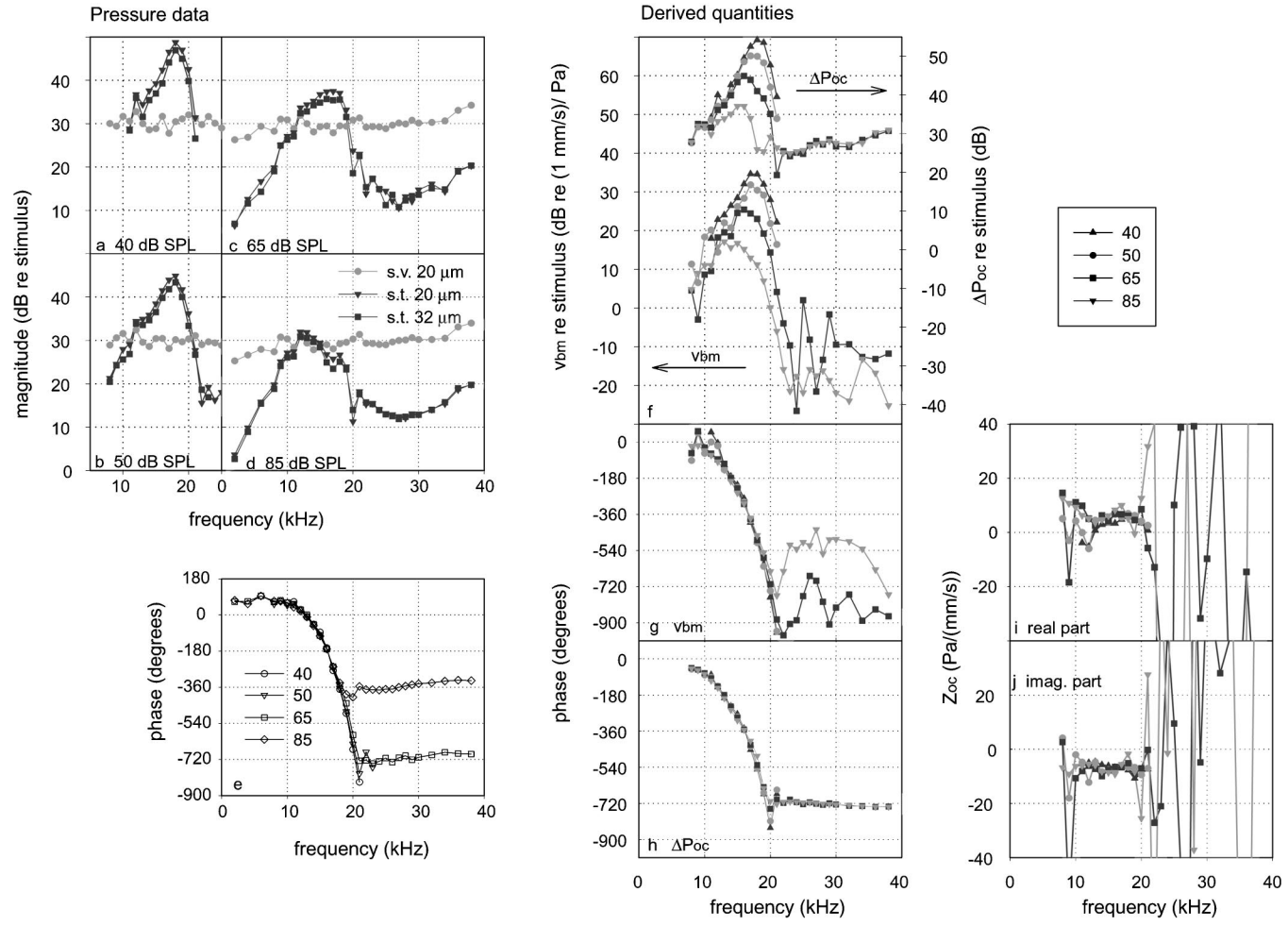

FIG. 19. Pressure data and derived quantities, 5-6-99. The analysis of this experiment used s.t. pressure data at the position not closest, but second closest to the b.m. because of the reversal in pressure magnitude that was described in Fig. 11. (a)–(e) The s.t. and s.v. pressures for impedance calculation. Magnitudes are shown relative to the stimulus level in the ear canal; phases (s.t. only) are relative to the simultaneously measured s.v. pressure. Distances in the key refer to the distance between the b.m. and the s.t. sensor. (a) Magnitude, 40 dB SPL stimulus. (b) Magnitude, 50 dB. (c) Magnitude, 65 dB. (d) Magnitude, 85 dB. (e) Phase, all levels. (f)–(j) ΔP_{OC}, $v_{b.m.}$, and Z_{OC}. The usual calculation for ΔP_{OC} was used. (f) Magnitude of $v_{b.m.}$ and ΔP_{OC} (*re* stimulus level). (g) Phase of $v_{b.m.}$ *re* simultaneously measured s.v. pressure. (h) Phase of ΔP_{OC} re simultaneously measured s.v. pressure. (i) Real part of Z_{OC}. (j) Imaginary part of Z_{OC}.

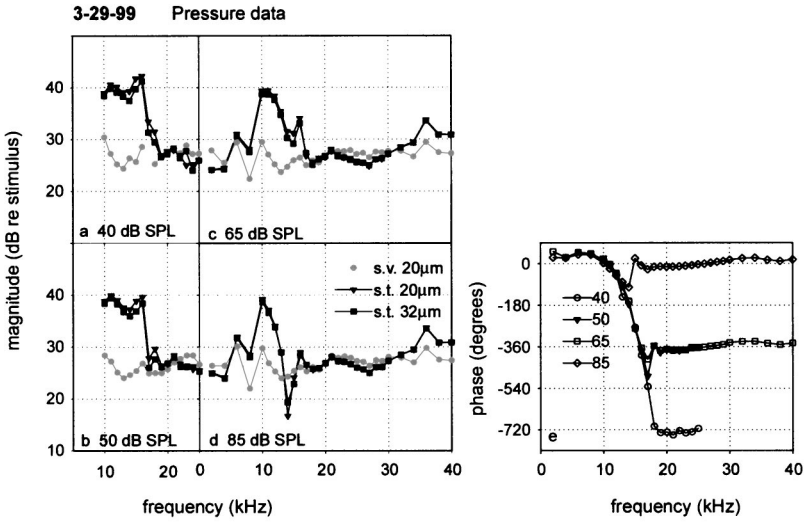

FIG. 20. Pressure data, 3-29-99. The s.t. and s.v. pressures for impedance calculation 3-29-99-usual and 3-29-99-double. The impedance analysis of this experiment used s.t. pressure data at the position not closest, but second closest to the b.m. because of a reversal in pressure magnitude at the closest position. Magnitudes are shown relative to the stimulus level in the ear canal; phases (s.t. only) are relative to the simultaneously measured s.v. pressure. Distances in the key refer to the distance between the b.m. and the s.t. sensor. (a) Magnitude, 40 dB SPL stimulus. (b) Magnitude, 50 dB. (c) Magnitude, 65 dB. (d) Magnitude, 85 dB. (e) Phase, all levels.

sis. The detections of negative resistance above agreed with deBoer and Nuttall's results in that a relatively small degree of nonlinear negative resistance at frequencies below the b.f. produced a large degree of nonlinearity in the response in the b.f. region. However, in the report of deBoer and Nuttall the region of negative resistance was broader, and more robust than in the current report. Notably, at the frequencies where they found negative resistance its magnitude was at most 20%–30% of the magnitude of the imaginary part of the impedance. These robust detections occurred at low stimulus levels in very sensitive cochleae. If this is true, negative resistance will be challenging to detect decisively with the more direct approach of the present study.

The results of de Boer and Nuttall (1999) and those of the present report agree on other points as well. In both reports well beneath the b.f. (basal to the peak) the real part and imaginary part of the impedance were usually within ~ a factor of 2 to each other in magnitude. In both reports even

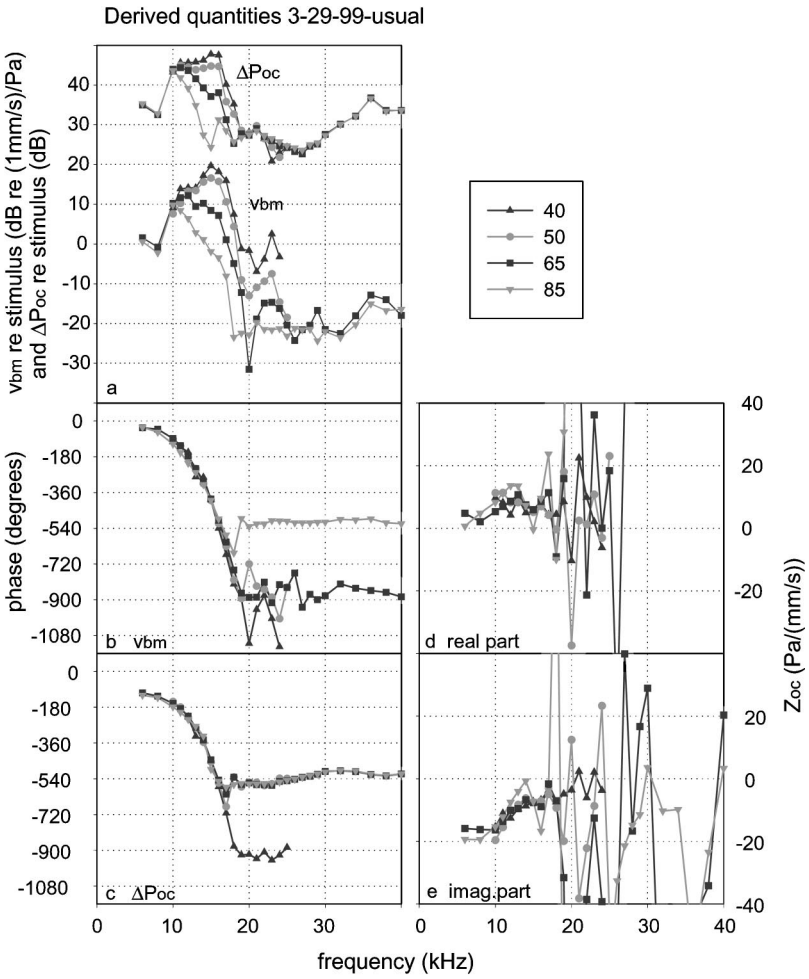

FIG. 21. Derived quantities, ΔP_{OC}, $v_{b.m.}$, and Z_{OC}, 3-29-99-usual. The usual calculation for ΔP_{OC} was used. (a) Magnitude of $v_{b.m.}$ and ΔP_{OC} (*re* stimulus level). (b) Phase of $v_{b.m.}$ *re* simultaneously measured s.v. pressure. (c) Phase of ΔP_{OC} *re* simultaneously measured s.v. pressure. (d) Real part of Z_{OC}. (e) Imaginary part of Z_{OC}.

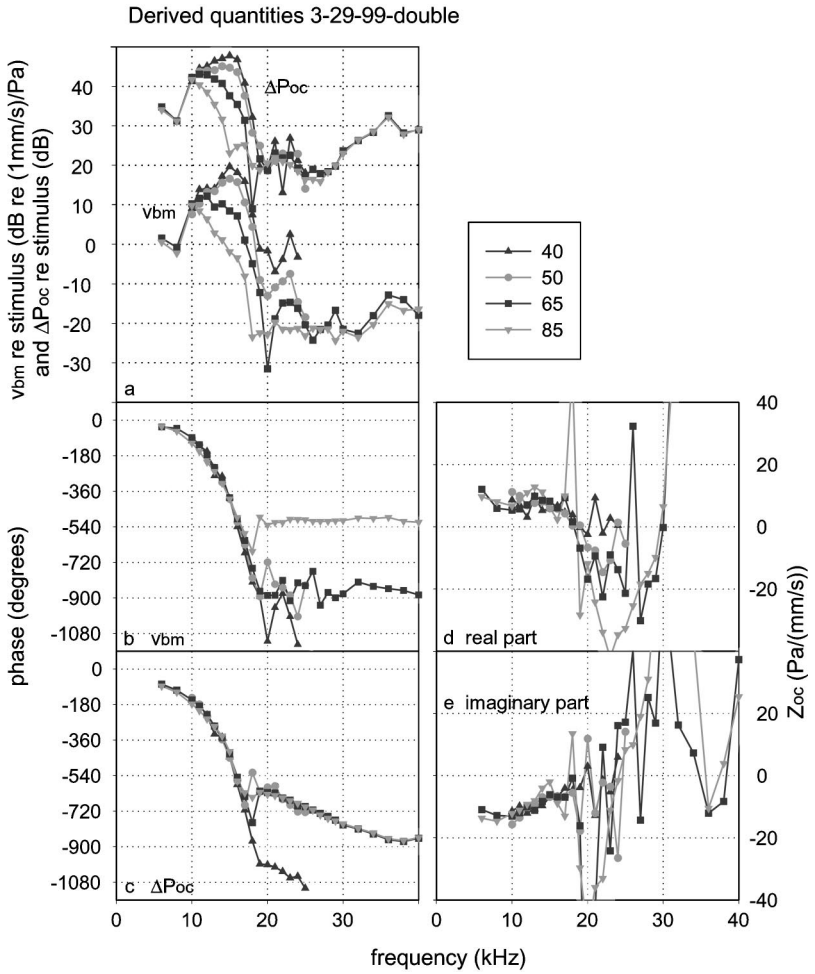

FIG. 22. Derived quantities, ΔP_{OC}, $v_{b.m.}$, and Z_{OC}, 3-29-99-double. The contribution of $P_{s.v.}$ was twice what it is in the usual calculation for ΔP_{OC}. (a) Magnitude of $v_{b.m.}$ and ΔP_{OC} (*re* stimulus level). (b) Phase of $v_{b.m.}$ *re* simultaneously measured s.v. pressure. (c) Phase of ΔP_{OC} *re* simultaneously measured s.v. pressure. (d) Real part of Z_{OC}. (e) Imaginary part of Z_{OC}.

in passive cochleae the real part of the impedance varied substantially with frequency (place).

The question of whether Z_{OC} possesses a spring–mass resonance is fundamental. If it does, the frequency map of the cochlea is established primarily by the stiffness and mass of the OCC and at frequencies above the resonant frequency (a little above the b.f.) of a particular point the traveling wave is not present at all. Many cochlear models employ a resonant Z_{OC} (e.g., Neely and Kim, 1986; Peterson and Bogart, 1950; Kolston, 2000). If the spring–mass resonance does not exist the frequency map of the cochlea is established by the stiffness of the OCC and wavelength dependent changes in fluid mass. Z_{OC} never becomes masslike, and the traveling wave is small but present at frequencies well above the b.f. Many cochlear models do *not* contain a resonant Z_{OC}. Steele and colleagues in particular maintain that the OC mass should have very little effect on cochlear mechanics (e.g., Steele, 1999; Steele and Taber, 1981). (The argument against the OC mass playing a mechanical role is that most of the cells of the OC are soft and the fluid within the cells would move almost as it would if it was not enclosed within cells.)

Experimentally, there is nothing truly compelling either for or against resonance. In the present studies and broadly in the literature a phase plateau is present at frequencies above b.f. (e.g., Rhode, 1971). At first glance this seems like evidence that the traveling wave has stopped. However, the traveling wave mode need only be small compared with the compressive mode (or other nonpropagating modes) and a phase plateau will be observed. In the presented study spring–mass resonance was detected in the impedance phase in half the measurements, appearing in both linear and nonlinear cochleae. These detections were based on the presence of a stiffness-mass transition, which occurred where the phase plateau began. The strength of this detection was compromised by the fact that in the plateau region the analysis for ΔP_{OC} was susceptible to experimental inaccuracies. Moreover, to be convincing the resonance should be apparent in both the magnitude and phase and it was not apparent in the magnitude. The inverse method of deBoer and Nuttall (e.g., 1999) did not detect a resonance. Although one could argue that their frequency range was not extended high enough above the b.f. to address resonance their results appear to weigh in against it. There is experimental evidence from linear cochleae that speaks against resonance. In linear cochleae with drained scala tympani the b.f. shifted up by about half an octave (discussed in Steele and Taber, 1981; Patuzzi *et al.*, 1982). This is predicted if fluid mass, not organ of Corti mass, determined the location of the peak. A complementary observation is that of Cooper and Rhode (1995), who in measurements of b.m. motion in the apex of guinea pig cochleae found no difference in peak location or shape when the organ of Corti was removed.

This report concludes with further strategies for probing negative resistance and resonance in Z_{OC}. The question of

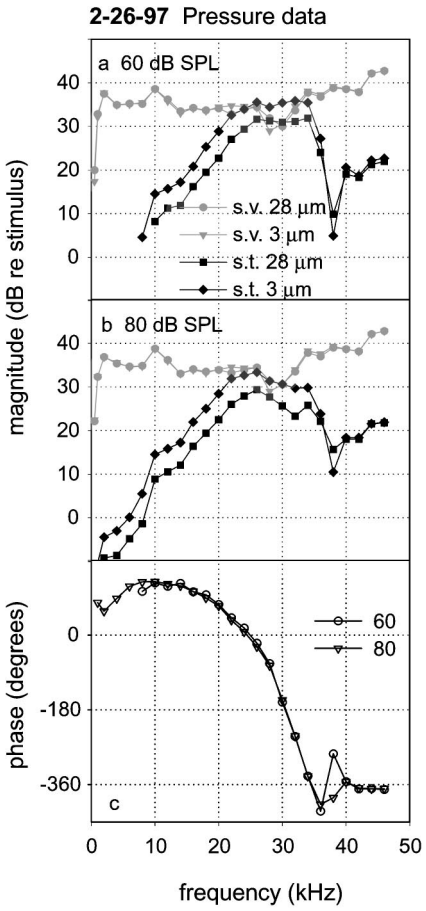

FIG. 23. Pressure data, 2-26-97. The s.t. and s.v. pressures for impedance calculation 2-26-97-usual and 2-26-97-half. This was an extreme basal experiment. Magnitudes are shown relative to the stimulus level in the ear canal; phases (s.t. only) are relative to the simultaneously measured s.v. pressure. Distances in the key refer to the distance between the b.m. and the s.t. sensor. (a) Magnitude, 60 dB SPL stimulus. (b) Magnitude, 80 dB. (c) Phase, both levels.

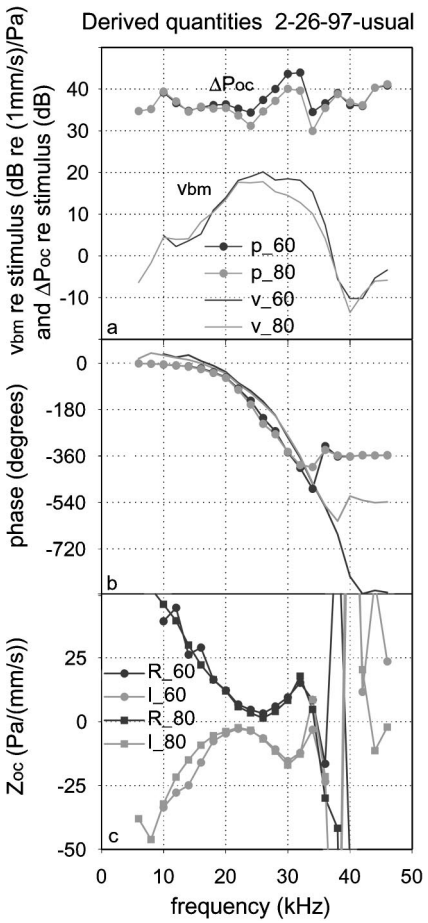

FIG. 24. Derived quantities, ΔP_{OC}, $v_{b.m.}$, and Z_{OC}, 2-26-97-usual. The usual calculation for ΔP_{OC} was used. (a) Magnitude of $v_{b.m.}$ and ΔP_{OC} (*re* stimulus level). (b) Phase of $v_{b.m.}$ and ΔP_{OC} (*re* simultaneously measured s.v. pressure). (c) Real and imaginary parts of Z_{OC}.

negative resistance might be explored via a more detailed map of the s.t. pressure. The impedance of the OCC influences the way that the fluid velocity varies with distance from the b.m. For example, in a simple two-dimensional (2D) system an impedance of stiffness is linked to an exponentially decreasing velocity-with-distance. However, a partly resistive impedance introduces oscillations into the exponential decrease (de Boer, 1984). The fluid velocity over a range of distances from the b.m. is measurable via pressure gradients (Olson, 1999). Such measurements, linked to a three-dimensional (3D) cochlear model might illuminate the question of negative resistance.

The resonance question might be explored via measurements of the longitudinal curvature of the traveling wave. Experimentally, curvature is found by taking the difference in b.m. motion phases ($\delta\phi$) between two locations spaced by a small longitudinal distance (δx). The curvature equals $\delta\phi/\delta x$ and is represented by the ''wave number,'' κ. The frequency dependence of the curvature depends on the organ of Corti mass (m_{OCC}, the OC mass/unit length) and fluid mass [$m_{eq}(\kappa)$, the equivalent mass of fluid/unit length which resists the displacement of the b.m. (Steele and Taber, 1979)]. These masses relate directly to resonance—resonance exists if and when m_{OCC} dominates $m_{eq}(\kappa)$ (Lighthill, 1981). $m_{eq}(\kappa)$ is prominent in many modeling papers [$m_{eq}(\kappa)$ is a scaled version of ''$h_{eq}(\kappa)$'' or ''$Q(\kappa)$'' found in, e.g., Steele and Taber, 1979; Lighthill, 1981; de Boer, 1984]. Its variation with κ is what distinguishes 1D, 2D, and 3D cochlear models. (In the following, ω is the angular frequency, z is the z displacement of the b.m. and s is the OCC stiffness/length at the longitudinal location of the measurement. As in most cochlear models, s is assumed independent of κ.)

By equating the potential and kinetic energies of the traveling wave at every longitudinal location the relationship between stiffness, mass and frequency is (Lighthill, 1983):

$$\tfrac{1}{2}sz^2 = \tfrac{1}{2}(m_{eq}(\kappa) + m_{OCC})\omega^2 z^2. \tag{5}$$

Experimentally measuring curvature at many frequencies leads to $\kappa(\omega)$, or equivalently, $\omega(\kappa)$. Equation (5) can be rewritten as

$$(m_{eq}(\kappa) + m_{OCC})/s = (\omega(\kappa))^{-2}. \tag{6}$$

The right-hand side of Eq. (6) is an experimental quantity, so the left-hand side is experimentally accessible. The idea is to find how the wave curvature varies with frequency in the region of the peak, and to use the result to ''measure'' $(m_{eq}(\kappa) + m_{OCC})/s$ vs κ. Does it begin to level off to a con-

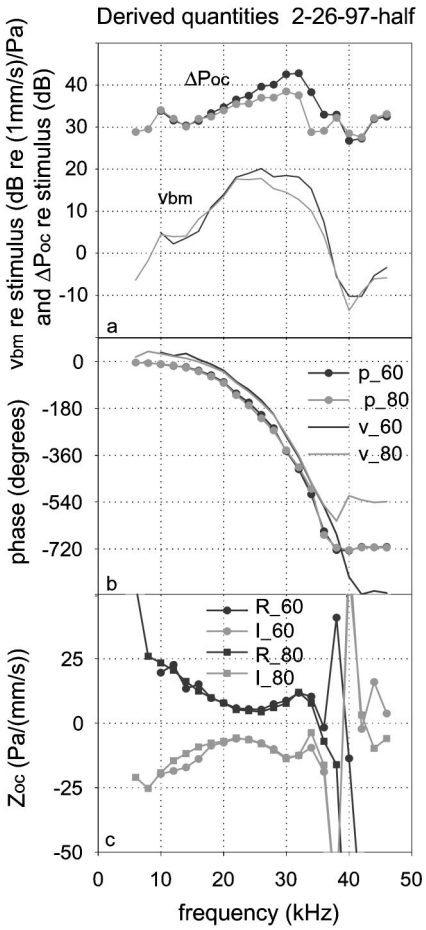

FIG. 25. Derived quantities, ΔP_{OC}, $v_{b.m.}$, and Z_{OC}, 2-26-97-half. The contribution of $P_{s.v.}$ was half what it is in the usual calculation for ΔP_{OC}. (a) Magnitude of $v_{b.m.}$ and ΔP_{OC} (*re* stimulus level). (b) Phase of $v_{b.m.}$ and ΔP_{OC} (*re* simultaneously measured s.v. pressure). (c) Real and imaginary parts of Z_{OC}.

stant value? (If yes, resonance is supported.) Does it look just like $m_{eq}(\kappa)$ from 3D cochlear models looks, so m_{OCC} is effectively zero? (If yes, resonance is contested.) Lighthill (1981) examined Rhode's (1971) measurements, longitudinally spaced by 1.5 mm, and decided that the variation of ω with κ was consistent with the presence of resonance. However, more closely spaced longitudinal measurements, such as have been appearing in the experimental literature (Russell and Nilson, 1997; Ren, 2001; Rhode and Recio, 2000) are better for measuring curvature and for addressing the question of resonance.

ACKNOWLEDGMENTS

This work was supported by NIH DC03130. Many thanks to Egbert deBoer, Hideko Nakajima and the J. Acoust. Soc. Am. reviewers, Chris Shera and ''A'' for improving the presentation.

[1]This derives from a simplification of the Navier–Stokes equation, $\nabla P = -\rho \partial v/\partial t - \rho v \nabla v + \mu \nabla^2 v$. The equation can be approximated as $\nabla P = -\rho \partial v/\partial t$ at high enough frequencies. In Olson (1998) the relative sizes of the three right-hand terms was approximated using dimensional analysis. The length scale over which fluid velocity changed by $\sim$ a factor of e was estimated as 100 μm. Then at 1.5 kHz the first right-side term was 1000 times bigger than the second term and 100 times bigger than the third term. The dominance of the first term grows with frequency. However, in recent measurements close to the b.m. the length over which the velocity dropped off by a factor of e was found to be only 15 μm (Olson, 1999). This reduced length scale reduced the dominance of the first term; at 3.5 kHz, it is 300 times bigger than the second term and 5 times bigger than the third term. Therefore, the method to find fluid velocity close to the b.m. using Eq. (2) is restricted to frequencies over several kHz.

[2]With a symmetric cochlear model, the pressure can be decomposed into symmetric and antisymmetric parts (Peterson and Bogart, 1950). For simplicity the derivation above only discussed the antisymmetric part. Including the symmetric component does not change the answer as long as the symmetric component does not vary spatially. The symmetric component is associated with the compressional wave. It is expected to vary in space

TABLE I. Summary of impedance results from six experiments. Symbols in the table refer to the following notes: *Results ambiguous, see discussion. †Roman numerals I and II in expt 9-8-98 refer to two different approaches. The suffixes half, double, and usual are appended when alternative calculations for ΔP_{OC} were done. §During the first approach of expt. 9-8-98, two pressure series were actually taken, separated by more than an hour in time, but without repositioning the sensor. The results of these two series tested repeatability. They were similar and in particular both showed negative resistance. Only one of these is presented here (9-8-98-I). In a separate approach (9-8-98-II) the sensor was angled relative to the first by about 15° so that it would contact the b.m. $\sim$100 μm from the first approach in a direction towards the lamina. Because this approach found larger s.t. pressures the sensor was probably more radially and/or perpendicularly centered on the b.m. then.

Experiment date and region	Nonlinear experiment?	Measurement and analysis name†	Figure numbers	Negative resistance?	Spring–mass resonance? (apparent in phase)
12-10-98 turn one	no (or just barely)	12-10-98	12	no	yes
3-22-99 turn one	no (or just barely)	3-22-99	13	no	yes
9-8-98 turn one§	yes	9-8-98-I-usual	14,15	yes	yes
		9-8-98-I-half	14,16	yes	no
		9-8-98-I-double	14,17	*	yes
		9-8-98-II	18	no	no
5-6-99 turn one	yes	5-6-99	19	yes	*
3-29-99 turn one	yes, somewhat	3-29-99-usual	20,21	*	no
		3-29-99-double	20,22	no	no
2-26-97 extreme base	no (or just barely)	2-26-97-usual	23,24	no	no
		2-6-97-half	23,25	no	no

much more slowly than the antisymmetric part (Lighthill, 1981) and in the section on pressure versus position this was confirmed. Therefore, it can be considered as an offset, P_c. The antisymmetric part satisfies $P'_{\text{s.v.}} - P'_{\text{s.v.–OCC}} = P'_b - P'_{\text{r.w.}}$, but these primed quantities are no longer the actual pressure at each of these positions. Adding P_c to each term returns it to a form that includes actual pressures: $(P'_{\text{s.v.}}+P_c)-(P'_{\text{s.v.–OCC}}+P_c) = (P'_b+P_c)-(P'_{\text{r.w.}}+P_c)$ [equation (i)]. $(P'_{\text{s.v.}}+P_c)$ is the pressure measured in the s.v. $(P_{\text{s.v.}})$, (P'_b+P_c) is the s.t. pressure measured close to the b.m. (P_b). Because of the r.w. boundary condition $(P'_{\text{r.w.}}+P_c)=0$ [equation (ii)]. The desired quantity is $\Delta P_{\text{OC}}=(P'_{\text{s.v.–OCC}}+P_c)-(P'_b+P_c)$. From Eqs. (i) and (ii), $\Delta P_{\text{OC}}=(P'_{\text{s.v.}}+P_c)-2(P'_b+P_c)=P_{\text{s.v.}}-2P_b$, just as in Eq. (3).

Aibara, R., Welch, J., Puria, S., and Goode, R. L. (**1999**). ''Direct measurement of cochlear input impedance in human cadaver ear,'' Abstracts of the 2nd International Symposium of Middle-ear Mechanics in Research and Otosurgery, Boston, MA.

Avan, P., Magnan, P., Smurzynski, J., Probst, R., and Dancer, A. (**1998**). ''Direct evidence of cubic difference tone propagation by intracochlear acoustic pressure measurements in the guinea-pig,'' Eur. J. Neurosci. **10**, 1764–1770.

Beranek, L. L. (**1954**). *Acoustics* (Acoustical Society of America, 1996), Chap. 3.

Cooper, N. P. (**1998**). ''Harmonic distortion on the basilar membrane in the basal turn of the guinea-pig cochlea,'' J. Physiol. (Paris) **509**, 277–288.

Cooper, N. P. (**2000**). ''Radial variation in the vibrations of the cochlear partition,'' in *Recent Developments in Auditory Mechanics*, edited by H. Wada, T. Takasaka, K. Ikeda, K. Ohyama, and T. Koike (World Scientific, Singapore), pp. 109–115.

Cooper, N. P., and Rhode, W. S. (**1995**). ''Nonlinear mechanics at the apex of the guinea-pig cochlea,'' Hear. Res. **82**, 225–243.

Cooper, N. P., and Rhode, W. S. (**1996**). ''Fast traveling waves, slow traveling waves, and their interactions in experimental studies of apical cochlear mechanics,'' Aud. Neurosci. **2**, 207–212.

Crawford, A. C., and Fettiplace, R. (**1981**). ''An electrical tuning mechanism in turtle cochlear hair cells,'' J. Physiol. (London) **312**, 377–412.

Dancer, A., and Franke, R. (**1980**). ''Intracochlear sound pressure measurements in guinea pigs,'' Hear. Res. **2**, 191–205.

de Boer, E. (**1983**). ''No sharpening? A challenge for cochlear mechanics,'' J. Acoust. Soc. Am. **73**, 567–573.

de Boer, E. (**1984**). ''Auditory physics. Physical principles in hearing theory. II,'' Phys. Rep. **105**, 141–226.

de Boer, E., and Nuttall, A. L. (**1999**). ''The inverse problem solved for a three-dimensional model of the cochlea. III. Brushing-up the solution method,'' J. Acoust. Soc. Am. **105**, 3410–3420.

de Boer, E., and Nuttall, A. L. (**2000**). ''The mechanical waveform of the basilar membrane. III. Intensity effects,'' J. Acoust. Soc. Am. **107**, 1497–1507.

Decory, L., Franke, R. B., and Dancer, A. L. (**1990**). ''Measurement of middle ear transfer function in cat, chinchilla and guinea pig,'' in *The Mechanics and Biophysics of Hearing*, edited by P. Dallos, C. D. Geisler, J. W. Matthews, M. A. Ruggero, and C. R. Steele (Springer-Verlag, Berlin), pp. 270–277.

Freeman, D. M., and Weiss, T. F. (**1990**). ''Hydrodynamic analysis of a two-dimensional model for micromechanical resonance of free-standing hair bundles,'' Hear. Res. **48**, 37–68.

Johnstone, J. R., Alder, V. A., Johnstone, B. M., Robertson, D., and Yates, G. K. (**1979**). ''Cochlear action potential threshold and single unit threshold,'' J. Acoust. Soc. Am. **65**, 254–257.

Kolston, P. J. (**2000**). ''The importance of phase data and model dimensionality to cochlear mechanics,'' Hear. Res. **145**, 25–36.

Kolston, P. J. (**1999**). ''Comparing *in vitro*, *in situ*, and *in vivo* experimental data in a three-dimensional model of mammalian cochlear mechanics,'' Proc. Natl. Acad. Sci. U.S.A. **96**, 3676–3681.

Lighthill, J. (**1981**). ''Energy flow in the cochlea,'' J. Fluid Mech. **106**, 149–213.

Lighthill, J. (**1983**). ''Advantages from describing cochlear mechanics in terms of energy flow,'' in *Mechanics of Hearing*, edited by E. de Boer and M. A. Viergever (Delft University Press), pp. 63–71.

Lynch, T. J., Nedzelnitsky, V., and Peake, W. T. (**1982**). ''Input impedance of the cochlea in cat,'' J. Acoust. Soc. Am. **72**, 108–123.

Magnan, P., Avan, P., Dancer, A., Probst, R., and Smurzynski, J. (**1997**). ''A new approach to cochlear mechanics and cubic distortion tones by intracochlear acoustic pressure measurements in the guinea pig,'' in *Diversity in Auditory Mechanics*, edited by E. R. Lewis, G. R. Long, R. F. Lyon, P. M. Narins, C. R. Steele, and E. Hecht-Poinar (World Scientific, Singapore), pp. 333–338.

Magnan, P., Dancer, A., Probst, R., Smurzynski, J., and Avan, P. (**1999**). ''Intracochlear acoustic pressure measurements: Transfer functions of the middle ear and cochlear mechanics,'' Aud. Neurootol. **4**, 123–128.

Mountain, D. C., and Hubbard, A. E. (**1989**). ''Rapid force production in the cochlea,'' Hear. Res. **42**, 195–202.

Narayan, S. S., and Ruggero, M. A. (**2000**). ''Basilar membrane mechanics at the hook region of the chinchilla cochlea,'' in *Recent Developments in Auditory Mechanics*, edited by H. Wada, T. Takasaka, K. Ikeda, K. Ohyama, and T. Koike (World Scientific, Singapore), pp. 95–101.

Nedzelnitsky, V. (**1980**). ''Sound pressures in the basal turn of the cat cochlea,'' J. Acoust. Soc. Am. **68**, 1676–1689.

Neely, S. T., and Kim, D. O. (**1986**). ''A model for active elements in cochlear biomechanics,'' J. Acoust. Soc. Am. **79**, 1472–1480.

Nilsen, K. E., and Russell, I. J. (**1999**). ''Timing of cochlear feedback: spatial and temporal representation of a tone across the basilar membrane,'' Nat. Neurosci. **2**, 642–648.

Olson, E. S. (**1998**). ''Observing middle and inner ear mechanics with novel intracochlear pressure sensors,'' J. Acoust. Soc. Am. **103**, 3445–3463.

Olson, E. S. (**1999**). ''Direct measurement of intracochlear pressure waves,'' Nature (London) **402**, 526–529.

Olson, E. S. (**2000**). ''The use of intracochlear pressure to find the impedance of the organ of Corti,'' in *Recent Developments in Auditory Mechanics*, edited by H. Wada, T. Takasaka, K. Ikeda, K. Ohyama, and T. Koike (World Scientific, Singapore), pp. 144–150.

Olson, E. S., and Mountain, D. C. (**1991**). ''In vivo measurement of basilar membrane stiffness,'' J. Acoust. Soc. Am. **89**, 1262–1275.

Olson, E. S., and Cooper, N. P. (**2000**). ''Stapes motion and scala vestibuli pressure in gerbil,'' Abstract #4415 from the Midwinter Meeting of the Association for Research in Ololaryngology.

Patuzzi, R., Sellick, P. M., and Johnstone, B. M. (**1982**). ''Cochlear drainage and basilar membrane tuning,'' J. Acoust. Soc. Am. **72**, 1064–1065.

Peterson, L. C., and Bogart, B. P. (**1950**). ''A dynamical theory of the cochlea,'' J. Acoust. Soc. Am. **22**, 369–381.

Puria, S., and Rosowski, J. J. (**1997**). ''Measurement of reverse transmission in the human middle ear: preliminary results,'' in *Diversity in Auditory Mechanics*, edited by E. R. Lewis, G. R. Long, R. F. Lyon, P. M. Narins, C. R. Steele, and E. Hecht-Poinar (World Scientific, Singapore), pp. 151–157.

Puria, S., Peake, W. T., and Rosowski, J. J. (**1997**). ''Sound-pressure measurements in the cochlear vestibule of human-cadaver ears,'' J. Acoust. Soc. Am. **101**, 2754–2769.

Ren, T. (**2001**). ''Direct measurement of the traveling wave using a scanning laser interferometer in sensitive gerbil cochlea,'' Abstract #555 from the Midwinter Meeting of the Association for Research in Ololaryngology.

Rhode, W. S. (**1971**). ''Observations on the vibration of the basilar membrane in squirrel monkey using the Mössbauer technique,'' J. Acoust. Soc. Am. **49**, 1218–1231.

Rhode, W. S., and Recio, A. (**2000**). ''Study of mechanical motions in the basal region of the chinchilla cochlea,'' J. Acoust. Soc. Am. **107**, 3317–3332.

Ruggero, M. A., Rich, N. C., Robles, L., and Bhagyalakshmi, G. S. (**1990**). ''Middle ear response in the chinchilla and its relationship to mechanics at the base of the cochlea,'' J. Acoust. Soc. Am. **87**, 1612–1629.

Ruggero, M. A., Rich, N. C., Recio, A., Narayan, S. S., and Robles, L. (**1997**). ''Basilar membrane responses to tones at the base of the chinchilla cochlea,'' J. Acoust. Soc. Am. **101**, 2151–2163.

Russell, I. J., and Nilsen, K. E. (**1997**). ''The location of the cochlear amplifier: Spatial representation of a single tone on the guinea pig basilar membrane,'' Proc. Natl. Acad. Sci. U.S.A. **94**, 2660–2664.

Steele, C. R., and Taber, L. A. (**1979**). ''Comparison of WKB calculations and experimental results for three-dimensional cochlear models,'' J. Acoust. Soc. Am. **65**, 1007–1018.

Steele, C. R., and Taber, L. A. (**1981**). ''Three-dimensional model calculations for guinea pig cochlea,'' J. Acoust. Soc. Am. **69**, 1107–1111.

Steele, C. R. (**1999**). ''Toward three-dimensional analysis of cochlear structure,'' ORL **61**, 238–251.

Zwislocki, J. (**1965**). ''Analysis of some auditory characteristics,'' in *Handbook of Mathematical Psychology, Vol. III*, edited by R. D. Luce, R. R. Bush, and E. Galanter (Wiley, New York), pp. 3–97.